Annals of Nuclear Energy 160 (2021) 108436
https://doi.org/10.1016/j.anucene.2021.108436

Improvements of RELAP5/Mod3.3 heat transfer capabilities for simulation of in-pool passive power removal systems

Vincenzo Narcisi[1]*, Lorenzo Melchiorri[1], Fabio Giannetti[1]

[1]DIAEE – Nuclear Section, "Sapienza" University of Rome, Corso Vittorio Emanuele II, 244, 00186, Rome, Italy

*Corresponding author

Abstract

Despite system thermal-hydraulic codes were extensively validated for transient simulations of LWR, several activities highlighted limited capabilities of these tools to model heat transfer within in-pool passive power removal system. Discrepancies with experimental results were related to the underestimate of pool boiling and film condensation heat transfer coefficients. Thus, the DIAEE of "Sapienza" University of Rome developed a modified version of RELAP5/Mod3.3, able to handle fundamental heat exchange phenomena involved in passive in-pool safety systems. A primary validation procedure has been performed for separated and integral effects. Dealing with nucleate boiling, the Root Mean Squared Relative Error (RMSRE) of wall superheat has been reduced from 1.290 to 0.182. Concerning film condensation, wall temperature RMSRE has been reduced from 0.192 to 0.058. The integral effect assessment has involved an experimental test of the PERSEO facility. The qualitative comparison between experiments and calculations has highlighted significant improvements of the modified RELAP5/Mod3.3.

Keywords

Safety system, PERSEO experiment, nucleate boiling, pool boiling, film condensation, heat transfer coefficient.

1 Introduction

The Fukushima Daiichi reactor accident drastically affected the development of the advanced Nuclear Power Plants (NPPs). As matter of fact, it showcased the critical issues that the so-called "Generation II" reactors own, whenever prolonged loss of external electricity events must be handled. In such NPPs, safety functions rely on active systems that require external power to fulfil their operation. This is the reason why, the Extended Loss of AC Power (ELAP) event occurred at Fukushima Daiichi NPP, led to a severe accident which jeopardized the plant functioning.

As a consequence of that dramatic event, the nuclear power industry focused its efforts on developing and designing passive safety systems. Exploiting fundamental physical principles (e.g., natural circulation and gravity), a passive safety system reduces the chance and the magnitude of core damage, that could derive from an ELAP event. Moreover, passive safety systems are beneficial for the project cost of the NPPs, minimizing the number of active equipment. Thus, safety and economic enhancements encouraged designers to implement passive safety systems in those reactors already equipped with active safety devices. Such procedure has been

Annals of Nuclear Energy 160 (2021) 108436
https://doi.org/10.1016/j.anucene.2021.108436

applied for the Advanced Power Reactor Plus (APR+) (Bae et al., 2012; Kang et al.,2012) and the HPR1000 (Xing et al., 2016; Xiaofan et al., 2017). The integration of passive systems has successfully increased the safety of these reactors; however, the capability to mitigate the consequences of an ELAP scenario is still limited by the presence of active components. For this reason, advanced reactors development foresees the employment of safety passive systems only, to guarantee the most efficient mitigation of severe accidents consequences. Examples of passive NPPs are: the AP1000 (Schulz, 2006; Jiang et al., 2017), the Economic Simplified Boiling Water Reactor (ESBWR) (Challberg et al., 1998; Rassame et al., 2017), the Advanced Heavy Water Reactor (AHWR) (Jain et al., 2013; Dasgupta et al., 2017) and the innovative Power Reactor (iPOWER) (Lee et al., 2017; Kang et al., 2019). Moreover, the interest for passive safety systems is confirmed in the so-called Generation IV (GEN-IV) reactors, as the Advanced Lead Fast Reactor European Demonstrator (ALFRED) (Alemberti et al., 2020). In a Lead-cooled Fast Reactors (LFRs) (more in general, in liquid metal-cooled NPPs), the Decay Heat Removal (DHR) system must ensure core cooling while avoiding lead freezing. The suitable solution proposed for ALFRED consists of a passive regulation of the exchanged power, performed by the Isolation Condenser (IC) (Caramello et al., 2017; Narcisi et al., 2020a).

According to the International Atomic Energy Agency (IAEA) standards, it is allowed to operate a passive system with a single action of an active component (e.g., opening a valve), using an independent stored source (IAEA, 2016). In this framework, a full-scale in-pool heat exchanger was designed and tested in a collaboration between the Italian National Agency for New Technologies, Energy and Sustainable Economic Development (ENEA) and SIET laboratories. The in-Pool Energy Removal System for Emergency Operation (PERSEO) facility consists of a Heat eXchanger (HX), fed with high-pressure steam while submerged in a water pool at atmospheric conditions. The system comes into operation whenever a dedicated valve on the secondary side is opened (Ferri et al., 2005).

The experimental campaign performed in PERSEO facility, promoted in first instance to assess the performance of a full-scale in-pool heat exchanger, has also been employed as benchmark exercise for best estimate System Thermal-Hydraulic (STH) codes. Indeed, many of those computational tools were extensively validated for a wide range of scenarios involving only active systems. Is crucial to underline that validation of best estimate STH codes is an essential step for the assessment of safety and reliability of passive systems. In this context, a benchmark was proposed within the OECD/NEA/CSNI/WGAMA “Thermal-hydraulics of passive safety systems in water-cooled reactors” exerting data from an experimental campaign carried out on PERSEO facility (Mascari et al., 2020). One of the most relevant outcomes was that the codes involved in the activity (twelve institutions took part in the benchmark with eleven different codes) effectively reproduced the overall experimental features. Nevertheless, most of them showed a relevant underestimate of the heat exchange between the HX and the HXP. However, the open nature of the benchmark allowed the participants to tune their models to overcome such drawbacks (Mascari et al., 2020).

The Department of Astronautical, Electrical and Energy Engineering (DIAEE) of “Sapienza” University of Rome took part in the validation benchmark using RELAP5-3D©. The authors assessed the limitations of the code to model a passive in-pool heat exchanger, that as mentioned before, consist in a poor prediction of heat transfer phenomena occurring (Narcisi et al., 2020b). This evidence motivated the authors to start a developing activity on the RELAP5/Mod3.3 (R5) code, optimizing the capabilities of the numerical tool in order to better simulate such a passive safety system.

Several works are found in literature dealing with the application of different versions of RELAP5 for the simulation of PERSEO experimental tests. Still, similar outcomes were found by different researchers, namely, that the heat transfer model between HX and pool must be refined (Ferri et al., 2005; Narcisi et al., 2020b;

Annals of Nuclear Energy 160 (2021) 108436
https://doi.org/10.1016/j.anucene.2021.108436

Bianchi et al., 2004; Bersano et al., 2020). Narcisi et al. (2020b) focused the attention on the evaluation of the Heat Transfer Coefficient (HTC) in pool boiling and in condensation within vertical tubes under low flow regime. In this specific application, the R5-3D default correlations exceeded their validity range, leading to the underestimate of the heat exchange. Two HTC multiplicative factors were derived, taking into account more adequate correlations. The enhancing factors assume the following values: 9 for pool boiling mechanism and 1.3 for condensation (applied to the Vierow and Schrock (1991) modification of the Nusselt model). Bersano et al. (2020) interrelated the considerable underrate of the heat exchange to the condensation HTC. They analysed different sets of correlation to improve the HTC esteem, deriving an enhancing HTC factor of 3.54, applied to the Nusselt model.

Although the application of HTC multiplicative factors allows a satisfactory prediction of the experimental data, it is not amenable to adopt this procedure in best-estimate calculations. Indeed, it is expected that the enhancing factors depend on several parameters (e.g., thermodynamic conditions and geometrical characteristics) thus, they are suitable just for a narrow range of study cases. Moreover, even though the same experiment has been involved, authors of abovementioned references disagree on the possible solution to overcome simulations flaw, proving the complexity of the problem. Therefore, the development alongside with the Verification and Validation (V&V) of a more suitable best estimate STH code for simulation of in-pool passive power removal systems is required. For this reason, in this work is presented a modified version of the RELAP5/Mod3.3 code, that is able to effectively process thermal-hydraulics phenomena occurring in those passive systems. At first, modifications made to the source code are introduced and then the V&V process is discussed.

2 State of the art and proposed modifications

The following section provides an overview on the state of art about important configurations for an in-pool passive heat exchanger, i.e., the pool boiling in cylindrical vertical geometry and the condensation within vertical tubes. Moreover, the original correlations implemented in the R5 default version and the proposed modifications are discussed.

2.1 Nucleate pool boiling on vertical tubes

Nucleate boiling is the most efficient heat transfer mechanism, hence it is extensively adopted in the passive heat removal systems for advanced NPPs. In literature, pool boiling effects in horizontal geometry are well characterized (Pioro et al., 2004; Jones et al., 2009). However, pool boiling on the outer surface of vertical tubes presents unique heat transfer features that must be addressed for a comprehensive knowledge of the phenomena occurring in a heat exchanger submerged in a water pool at atmospheric conditions.

Some experimental studies are available in the literature; most of them adopted vertical electrical heated rods to investigate the phenomenon at imposed heat flux. A notable example is the work performed by Kang (1998), where the impact of the pipe length on the nucleate pool boiling heat transfer is analysed. The experiment showed that the heat transfer rate decreases as the tube length increases. It is due to the larger bubble slug formation on the tube surface, which becomes relevant when the non-dimensional length (equal to the ratio between length and outer diameter) exceeds 50. When the mentioned value is overcome, the heat flux is observed to decrease linearly with the increase of the non-dimensional length. This effect is magnified as tube surface gets smoother (Kang, 1998). Consequently, the influence of surface roughness is examined in depth by Kang (2000), where a parametric study is provided in the range of 15.1 to 60.9 nm. The experiments showed that accreted surface roughness enhances heat transfer, since nucleation sites density grows. Furthermore, this

Annals of Nuclear Energy 160 (2021) 108436
https://doi.org/10.1016/j.anucene.2021.108436

phenomenon is amplified in vertical tubes, if compared to horizontal orientation. This is due to the grade of the liquid agitation, higher in vertical geometry, which determines less intense bubble coalescence (Kang, 2000). In general, the liquid agitation due to bubbles generation heightens the heat transfer, whereas the formation of large vapor slugs derived by bubble coalescence tends to reduce the heat exchange. The balance between these two heat transfer mechanisms is governed by the heat flux. As matter of fact, Chun and Kang (1998) observed that the degradation effect is more pronounced when heat flux is higher than 50 kW/m^2. This behaviour is emphasized for vertical tubes, where the coalescing bubbles are more equally distributed over the whole heating surface. Chun and Kang (1998) also assessed the influence of the tube diameter, verifying the heat transfer decreases as the diameter increases. It is found to be true for both vertical and horizontal geometries, but it is more relevant for the former.

Sateesh et al. (2009) further investigated the nucleate pool boiling on vertical tubes, taking in account the effect of surface roughness up to 0.67 μm. The test section used for the analysis was made by an electrically heated rod installed within a tank. Moreover, a tilting mechanism allowed to place the whole test section at different angles, for investigating the influence of tube inclination. The experimental campaign highlighted a weak impact on the average heat flux, especially for rougher surfaces. For what concerns local heat transfer, the most interesting result is the increase of the temperature at the top wall and a simultaneous decrease at the bottom, as the inclination differs from the vertical orientation. That is due to the more intense bubble coalescence at the top wall.

The main outcomes briefly discussed above, are confirmed by Gupta et al. (2010), who investigated the nucleate pool boiling over a bundle of vertical tubes. The test section consisted of a bundle of seven electrically heated rods (non-dimensional length around 42), arranged within a cylindrical tank. The experimental data were obtained in a heat flux range of 2-32 kW/m^2. It is highlighted that HTC on such tubes bundle increases with vertical length and the ratio between HTC at the top and at the bottom of the bundle is higher at low heat flux. Such evidence could seem in contradiction with results obtained by Kang (1998), but it should be noted that Kang (1998) experienced the degradation of the HTC along vertical dimension when non-dimensional length exceeds 50 and this effect is prominent when heat flux is greater than 50 kW/m^2 (Chun and Kang, 1998).

2.2 Film condensation in vertical tubes

The film condensation heat transfer in a vertical tube is an integral part of the passive safety systems designed for the advanced NPPs. In the present paper, focus is given to pure steam condensation within large tube diameter at high pressure. Typically, large diameters pipes are adopted in passive systems to limit pressure drops and promote natural circulation. Conversely, steam thermodynamic conditions depend on the design of the system. For example, the Simplified Boiling Water Reactor (SBWR) relies on a Passive Containment Cooling System (PCCS) alongside with an IC system. The two systems consist of vertical tubes heat exchangers (outer diameter is 50.8 mm) immersed in compartmentalized water pools. The PCCS operates at low pressure (0.31 MPa) while the IC system at high pressure (7.18 MPa) (Shumway, 1995).

There are few available data in the literature, concerning high-pressure steam condensation within vertical tubes characterized by large diameter. Kim and No (2000) investigated this phenomenon in the experiment carried out with a scaled facility composed of a vertical condenser tube (outer diameter of 50.8 mm) submerged in a water pool. A steam generator provided the steam which feeds the condenser. An overall number of 984 local data were collected, varying the steam pressure in a range of 0.35-7.2 MPa. The heat flux was found to increase with increasing pressure whereas the HTC was observed to keep a constant value, in the range of 4000-7000 W/m^{2}K.

Annals of Nuclear Energy 160 (2021) 108436
https://doi.org/10.1016/j.anucene.2021.108436

Moreover, other useful experiments were performed by Kuhn et al. (1997), despite they were performed at low pressures (0.1-0.5 MPa). As matter of fact, even if the present paper is focused on high pressure condensation, that experimental campaign provided useful peculiar information regarding steam condensation through vertical tubes, valid for both low and high pressure. Furthermore, it is worth emphasizing that modifications implemented in the code are suitable for a wide scale of pressure, therefore, they are comprehensive of the pressure ranges adopted in the aforementioned experiments. The test section was composed of a tube condenser surrounded by an annular cooling jacket. An overall number of 42 runs were carried out with pure steam. The experiment was focused on the characterization of the steam condensation within a vertical tube, adjusting the pressure in a range relevant for a PCCS and the steam flow rate in the range of 30-60 kg/h (Shumway, 1995; Kuhn et al., 1997).

2.3 RELAP5/Mod3.3 overview and proposed modifications

RELAP5/Mod3.3 is a one-dimensional thermal-hydraulic code developed in a collaboration between the U.S. Nuclear Regulatory Commission (NRC) and domestic organizations, members of the International Code Assessment and Application Program (ICAP) and the successor Code Applications and Maintenance Program (CAMP) (The RELAP5/Mod3.3 Code Development Team, 2003a). R5 was developed in Fortran environment. It is based on the non-homogeneous and non-equilibrium model for the two-phase system, solved by a fast, partially implicit numerical scheme that allows efficient calculation of system transient.

The code was originally designed and extensively validated for best-estimate transient simulation of Light Water Reactor (LWR) coolant system during operative transients and postulated accidents. The highly generic modelling approach allows to use this software for a wide variety of thermal-hydraulic systems.

In order to extend the code capabilities for both fusion reactors and advanced fission reactors applications, DIAEE, in collaboration with ENEA, are working on the development of an improved version of RELAP5/Mod3.3 (Giannetti et al., 2019). Currently, the enhancements implemented in the modified version of the numerical tool are thermophysical properties of new working fluids (i.e., lead and lead-bismuth eutectic alloy (Balestra et al., 2016), lithium-lead alloy (Martelli et al., 2018) and sodium-potassium alloy (Foust, 1972)), new HTC correlations and an additional subroutine for magnetohydrodynamics pressure drop evaluation (Melchiorri et al., 2021). Other groups work independently on improving of R5's capabilities. University of Pisa (Barone et al., 2019) and Xi'an Jiaotong University (Liu et al., 2017; 2018) has developed two versions including lithium-lead and others working fluids, and Kral (2015) implemented a specific heat transfer mode for condensation in horizontal and inclined tubes.

As reported in section 1, several examples in the literature point out the R5 significant underestimate of the heat transfer in a typical configuration of an IC system. Numerous researchers involved in these activities explained this behaviour with a defective calculation of the HTC for both the pool boiling and film condensation heat transfer (Mascari et al., 2020; Narcisi et al, 2020b). For this reason, the present activity aims to refine the code to provide a better evaluation of the HTC in such configurations.

The default version of the programme does not foresee a specific boundary condition type for nucleate pool boiling, employing the Chen correlation for the two-phase flow boiling HTC (Eq. (1)). This formulation is derived considering that heat transfer is governed by two mechanisms: the saturated nucleate boiling heat transfer and the single-phase forced convection (Chen, 1962; Chen, 1966; Chen and Fang, 2014):

$$h_{tp} = S \cdot h_{nb} + F \cdot h_{sp,f} \quad (1)$$

where the nucleate boiling h_{nb} is evaluated with the Forster and Zuber (1955) correlation for pool boiling (Eq. (2)) and the single-phase forced convection $h_{sp,l}$ is determined by the Dittus and Boelter (1985) correlation (Eq. (3)).

Annals of Nuclear Energy 160 (2021) 108436
https://doi.org/10.1016/j.anucene.2021.108436

$$h_{nb} = 0.00122\left(\frac{\lambda_f^{0.79} cp_f^{0.45} \rho_f^{0.49}}{\sigma^{0.5} \mu_f^{0.29} h_{fg}^{0.24} \rho_g^{0.24}}\right) \Delta T_{sat}^{0.24} \Delta p_{sat}^{0.75} \quad (2)$$

$$h_{sp,l} = 0.023 Re_f^{0.8} Pr_f^{0.4} \frac{\lambda_l}{D_H} \quad (3)$$

In Eq. (2), ΔT_{sat} stands for the excess between the wall temperature and the saturated temperature at the operating system and the Δp_{sat} is the difference between saturated pressure at the wall temperature and the operative pressure. In Eq. (3), Re_f denotes the Reynolds number for the liquid fraction of the mixture while the term Pr_f indicates the liquid Prandtl number. In Eq. (1), S is the suppression factor of the nucleate boiling whereas F stands for the two-phase correction factor of the single-phase forced convection. The parameter S approaches the unity whenever the two-phase Reynolds number $\left(Re_{tp} = Re_f \cdot F^{1.25}\right)$ is low (at low qualities and flow rates) and it decreases asymptotically to 0 at high Re. The factor F increases as the turbulence associated with two-phase flow increases (Chen and Fang, 2014).

As verified in the literature (see section 1), nucleate pool boiling depends on a wide variety of parameters (e.g., operating conditions, surface roughness, fluid properties). Forster and Zuber correlation, which was analytically derived, owns limited applicability since it neglects the surface effects (Jones et al., 2009). However, many correlations were formulated to handle a wide range of fluids and heater surfaces. Some of these require experimental data on the fluid-surface combination (e.g., Rohsenow (1952) correlation). Conversely, other correlations are independent by experimental data for the evaluation of nucleate pool boiling HTC, proving to be more useful for engineering applications. Relevant examples are given by Cooper (1984), Gorenflo (1993) and Leiner (1994).

The enhancement proposed in this paper is to include an additional correlation, more suitable for pool boiling heat transfer. For such thermal-hydraulic problem, Chen formulation is replaced with a new correlation which takes into account the surface characteristics. Among the available formulations, Cooper (1984) correlation has been selected. The rationale behind this choice is based on the single effect validation process and is discussed in section 3.1.1.

$$h = 55\left(p_r^{0.12-0.2\log_{10} R_{p,old}}\right)(-\log_{10} p_r)^{-0.55} M^{-0.5} q''^{0.67} \quad (4)$$

In Eq. (4), p_r is the reduced pressure, M is the molecular weight and q'' is the heat flux. The parameter $R_{p,old}$ represents the surface roughness (in μm) as defined by DIN 4762/1:1960. In its work, Cooper reformulated some correlations using the reduced properties, providing a simpler formulation without much loss in accuracy (Cooper, 1984). The final arrangement of the correlation (Eq. (4)) accounts for the effects of operating conditions, fluid properties and heater surface. About the surface roughness, Cooper based his analysis on the work of Nishikawa et al. (1982), which suggested that the effect of the surface roughness is greater at low pressure. Nishikawa et al. proposed a relationship between p_r and $R_{p,old}$ as $\left(8R_{p,old}\right)^{0.2(1-p_r)}$ but Cooper reformulates this term as $p_r^{0.12-0.2\log_{10} R_{p,old}}$.

Concerning the film condensation heat transfer, the default model of R5 (The RELAP5/Mod3.3 Code Development Team, 2003b) computes the HTC as the maximum of the Nusselt (1916) and the Shah (1979) correlations. The Nusselt theory for film condensation in vertical geometry is based on the local liquid film thickness, δ_z, and it is shown in Eq. (5):

$$h_{Nu,z} = \frac{k_f}{\delta_z} \quad (5)$$

The film thickness is expressed by the Eq. (6):

Annals of Nuclear Energy 160 (2021) 108436
https://doi.org/10.1016/j.anucene.2021.108436

$$\delta_z = 0.9086\left(\frac{\mu_f^2 Re'_f}{g\rho_f(\rho_f-\rho_g)}\right)^{\frac{1}{3}} \quad (6)$$

where *g* is the acceleration of gravity and Re'_f the condensate Reynolds number per unit width of the surface.

Dealing with the Shah formulation of the HTC, the default set of R5 adopts the first released correlation presented by Shah (1979). The correlation is shown in Eq. (7):

$$h_{Shah,1979} = h_{sp}\left(1+\frac{3.8}{Z^{0.95}}\right) \quad (7)$$

where h_{sp} stands for the HTC assuming liquid phase flowing alone in the tube (Eq. (8)) and *Z* indicates the Shah's correlating parameter defined in Eq. (9).

$$h_{sp} = h_{sp,l}(1-x)^{0.8} \quad (8)$$

$$Z = \left(\frac{1}{x}-1\right)^{0.8} p_r^{0.4} \quad (9)$$

In Eq. (8) and Eq. (9), *x* is the flow quality, calculated as the ratio between the steam/gas and the total mass flow rate, and $h_{sp,l}$ is defined by Eq. (3).

An additional model, proposed by Vierow and Schrock (1991), was tested in the past by Kuhn et al. (1997) and then implemented in R5-3D as an optional model. This formulation applied two corrective factors to the Nusselt equation. An enhancement factor accounts for the effect of the shear of the steam/gas phase on the liquid film while a suppression factor treats the non-condensable effects. The capability of this model to reproduce passive safety systems was assessed by Narcisi et al. (2020b), comparing R5-3D simulations with PERSEO experimental data. Although the optional model reduces the discrepancies between experiment and simulation, the improvement is not enough to provide a satisfactory estimation of the heat transfer.

The low accuracy of R5 in simulating film condensation in particular conditions have been mentioned in section 1. Bersano et al. (2020) questioned the applicability of Eq. (7) to model such passive safety systems, characterized by relatively large tube diameter. In this case, steam velocity is too low (around 2 m/s) and Nusselt HTC results higher than Shah formulation. Thus, Nusselt HTC is applied over the whole tube length, resulting in the miscalculate of the heat transfer (Bersano et al., 2020). Is worth noticing that Shah (1981) suggested to use Eq. (7) when the steam velocity exceeds 3 m/s. In addition, Papini and Cammi (2010) examined the applicability of Eq. (7) for high-pressure systems (e.g., IC system), proving the poor prediction of the HTC in these conditions.

Nevertheless, Shah (2009) reviewed Eq. (7) in a more recent study, optimizing the correlation. The objectives of that work were to extend the applicability of the formula to lowest flow rates and to widen the reduced pressure range. Shah identified three heat transfer regimes for vertical tubes, giving the following physical interpretation according to the condensate flow regimes: Regime III represents the laminar region, Regime I stands for the turbulent region, and Regime II is the transition region. For the laminar regime, Shah suggested to use the Nusselt equation (Eq. (5)) with the modification proposed by McAdams (1954) (increasing the HTC by 20%). For the turbulent regime, Shah proposed a revised version of Eq. (7):

$$h_{Shah,2009} = h_{sp}\left(1+\frac{3.8}{Z^{0.95}}\right)\left(\frac{\mu_f}{14\mu_g}\right)^{(0.0058+0.557p_r)} \quad (10)$$

Eq. (10) is the same as the previous version except for the viscosity ratio factor. Discrepancies at high reduced pressure were found to be related to the viscosity ratio of phases and the reduced pressure itself. This

correction factor was found to improve the agreement for both vertical and horizontal tubes. For the transition regime, Shah supposed that a satisfactory prediction of the heat transfer could be obtained by combining McAdams formulation with Eq. (10). A reasonable agreement with experimental data was found simply adding these two contributes.

After the three regimes have been defined, the boundaries between them must be set. For this purpose, Shah proposed an approach based on dimensionless parameters: the Shah's correlating parameter *Z* (Eq. (9)) and the dimensionless vapor volumetric flux, defined in Eq. (11).

$$J_g = \frac{xG}{\left(gD\rho_g(\rho_f - \rho_g)\right)^{0.5}} \tag{11}$$

In Eq. (11), *G* is the total mass flux and *D* is the inside tube diameter. Laminar regime occurs when the following condition is verified:

$$J_g \leq 0.89 - 0.93e^{(-0.087Z^{-1.17})} \tag{12}$$

Turbulent regime prevails when condition expressed by Eq. (13) is verified.

$$J_g \geq \frac{1}{2.4Z + 0.73} \tag{13}$$

If conditions defined by Eq. (12) and Eq. (13) are not verified, the transition regime occurs.

This methodology was in good agreement with experimental data of vertical tubes in a wide range of reduced pressure (between 0.0008 and 0.9) and of steam flow rate. Recently, Eq. (10) has been updated improving the boundaries definition for horizontal tubes (Shah, 2013) and HTC evaluation for mini/micro channels (Shah, 2016). Nevertheless, those changings do not affect the correlation efficacy for conventional vertical tubes.

Following Shah's suggestions, the authors have proposed a revision of the default set of correlations implemented in R5. For the turbulent regime, the correlations proposed by Shah in 1979 (Eq. (7)) is replaced with the more recent version shown in Eq. (10).For the laminar regime, Nusselt correlation (Eq. (5)) is kept, however, a clarification is necessary. According to some researchers, the 20% improvement of the Nusselt HTC in laminar condensation, discussed by McAdams (1954), may be due to the formation of waves in the liquid film (Guichet and Jouhara, 2020). Those fluctuations rearrange the fluid motion in a turbulent-like flow and, furthermore, reduce the average film thickness; for those reasons, the heat transfer is enhanced (Kapitza, 1948). This occurs for $Re'_f > 30$ (Rohsenow et al., 1998; Guichet and Jouhara, 2020). In order to consider the so called wavy laminar condensation heat transfer, Kutateladze (1963) proposed an alternative for the Nusselt correlations, resulting in Eq. (14):

$$h_{Kutateladze,z} = 0.69 Re'^{0.11}_f \cdot h_{Nu,z} \tag{14}$$

where Re'_f is the condensate Reynolds number per unit width of the surface.

Eq. (14) is added to the set of correlation for pure steam film condensation included in the R5 modified version. The HTC is calculated by the code as the maximum value among Eq. (5), Eq. (10) and Eq. (14). This approach is commonly used by R5 to guarantee a smooth transition between correlations (The RELAP5/Mod3.3 Code Development Team, 2003b). Besides, this assumption provides a satisfactory transition from laminar to wavy laminar regimes, since Eq. (14) results are greater than Eq. (5) for $Re'_f > 30$. Concerning the transition from wavy laminar to turbulent regimes, further investigations are required to assess the applicability of such methodologies. Nevertheless, it is worth noticing that Shah (2009) found a satisfactory agreement with

Annals of Nuclear Energy 160 (2021) 108436
https://doi.org/10.1016/j.anucene.2021.108436

experimental data simply adding the contribution of McAdams formulation with Eq. (10) within the transition regime.

3 Verification and validation

According to IAEA recommendations (IAEA, 2009), any computational tool or calculation method used in safety analysis shall undergo Verification and Validation (V&V) process to a sufficient agree. V&V procedure involves the review of the source coding and the assessment of the analytical models implemented in the code. It implies the comparison of the code predictions with experimental data and observation of actual systems.

As commonly stated (Glaeser,2017; IAEA, 2009), the objective of the verification is to prove whether the computational model correctly implements the intended conceptual and mathematical model and if physical equations have been properly implemented into the code. For this purpose, the verification process has been performed on the modified version of the code. At first, the original verification cases of Relap5 are repeated to ensure the original code capabilities are untouched. After that, new verification cases are employed to verify the proper working of the new implementations.

On the other hand, validation procedure must determine whether mathematical model is an accurate representation of the real system, by comparing simulation results with experimental acquisitions on real plants (Glaeser,2017; IAEA, 2009). In this study, code validation is pursued in two steps (Mascari et al., 2015). The first one is the single effect validation involving simple test cases. For this purpose, the experimental analyses presented by Sateesh et al. (2009) and Kuhn et al. (1997) are modelled with the modified version of R5 and the accuracy of the simulations is investigated. In the second step, the integral effect analysis is treated, reproducing an experimental test carried out in the PERSEO facility.

3.1 Single effect validation

3.1.1 Nucleate pool boiling

Among the experimental campaigns summarized in section 2.1, the experiment conducted by Sateesh et al. (2009) is selected for the V&V process. This choice is related to the characteristic of the test section and the available data found in the literature. Indeed, the experiment carried out by Kang and Chun (Kang, 1998; 2000; Chun and Kang, 1998) involves surface roughness (15.1 and 60.9 nm) that is extremely lower than the roughness of conventional tubes used in passive safety systems (around 1 μm). Moreover, information on surface roughness is not available for the experiments led by Gupta et al. (2010) hence, the work is not suitable for the validation phase.

The experimental facility of the selected campaign is fully described by Sateesh et al. (2009). It mainly consists of a boiling vessel, equipped with the vertical heating tube, a condenser, and their connections. The boiling vessel has the following dimensions: 120 mm x 120 mm x 300 mm. In addition to the main heating element, the boiling vessel is equipped with two secondary heaters (cartridge), installed sufficiently away from the main one. They operate to preheat the system and to maintain saturation condition during the test. A partially open valve ensures atmospheric condition within the tank. The boiling vessel is equipped with a tilting mechanism that allows to investigate the effect of the tube inclination. The main heating system is interchangeable. The examined test is characterized by a vertical heating tube with the outside diameter of 21 mm, active length of 172 mm (non-dimensional length: 8.2), surface roughness of 0.67 μm. Six Thermocouples (TCs) measures tube wall temperature at six different locations. The uncertainty of the TCs was ±0.1 K. Sateesh et al. (2009) determined the uncertainties of the limiting cases and derived the uncertainty related to the wall superheat,

Annals of Nuclear Energy 160 (2021) 108436
https://doi.org/10.1016/j.anucene.2021.108436

that was estimated to be ±3.5 %, and the uncertainty related to the heat flux, calculated by the method of propagation of error resulting in ±1%.

The modelling of the facility is limited to the boiling vessel and the main heating element. The pool is reproduced with two vertical parallel pipe components. One represents the inner volume, where the heating rod is installed, and the other one simulates the outer region of the tank. The total inventory of the pool is respected and the division of this parameter among the two pipe components was the subject of a mesh sensitivity analysis, that highlighted the independence between the heat transfer and the modelling choice. Thus, the total inventory is equally distributed in the two pipe components. Each one is composed of four Control Volumes (CVs), characterized by the axial length ranging between 64 and 86 mm and flow area along vertical axis of 7027 mm^2. The sliced modelling approach is adopted in the definition of the axial mesh. Four cross junctions connect the parallel pipes at each axial level, calculating the flow area as the lateral dimension of the pool (i.e., 120 mm) times the axial length of each CV. This methodology allows the reproduction of buoyancy within the tank (Narcisi et al., 2019). At the top, a time-dependent volume, connected to the upper surface of one pipe component, sets atmospheric conditions. The heating element is simulated with two heat structures thermally coupled with the two bottom CVs of one pipe component. Cylindrical geometry is chosen for the definition of the heat structures and actual geometrical features of the experimental apparatus are kept. The uniform heat flux flowing from the tube towards the pool is imposed as a boundary condition. Saturated conditions at atmospheric pressure are set as initial conditions for the calculations. Heat losses towards the environment are neglected since, in steady state, heat losses are balanced by the auxiliary heater, that is not modelled.

Four different steady state calculations have been performed using the default R5 and three versions of the code comprehensive of Cooper (1984), Gorenflo (1993) and Leiner (1994) correlations for pool boiling problems, respectively. Figure 1 compares the calculated wall superheat with the experimental acquisition. Among the proposed modifications, only Cooper's formulation is found to provide a relevant improvement on the estimate of the wall superheat. On the other hand, Gorenflo's correlation provides results comparable to the default R5, whereas Leiner's formulation fails in the prediction of the HTC, experiencing the largest discrepancy with experimental data. This is not surprising since the dependence between HTC and pressure was developed by Leiner (1994) specifically for fluids other than water. Hence, such correlation has been expected to not provide accurate predictions of water pool boiling.

Discrepancies between experiment and simulation grow with the heat flux, but they are satisfactory reduced using the Cooper correlation. Figure 2 shows a comparison of the experimental and calculated heat transfer coefficient. Concerning the experimental data, the heat transfer coefficient is evaluated with Eq. (15):

$$h = \frac{q''}{\Delta T_w} \tag{15}$$

where ΔT_w is the wall superheat. The uncertainty, evaluated with the propagation method, is estimated equal to ±4.5%.

The Root Mean Squared Relative Error (RMSRE) is used to assess the predictive capabilities of the codes. The RMSRE is calculated as:

$$RMSRE\ (\%) = 100 \cdot \sqrt{\frac{1}{N}\sum_{i=1}^{N}\left(\frac{y_{s,i} - y_{e,i}}{y_{e,i}}\right)^2} \tag{16}$$

Annals of Nuclear Energy 160 (2021) 108436
https://doi.org/10.1016/j.anucene.2021.108436

where y is the quantity (ΔT_w or h in this case) in the ith observation, N is the total number of observation and subscripts s and e stand respectively for simulation and experiment. The RMSREs of wall superheat and heat transfer coefficient are summarized in Table 1 and compared with experimental uncertainties.

Analogous results are obtained considering lower surface roughness, albeit discrepancy with experimental data is found to increase. The default version of the code does not account for the roughness effect, leading to an error amplification at low roughness. Concerning the improved version, it should be noted that Cooper correlation was verified within a relatively small range of roughness. Thus, the validity of this correlation for values lower than 0.02 µm should require a dedicated analysis.

Table 1. Nucleate pool boiling: summary of measurement uncertainties and calculated RMSRE (%)

	ΔT_w	h
Measurement uncertainty	3.5	4.5
Default R5	129.0	55.5
Modified R5: Cooper	18.2	15.3
Modified R5: Gorenflo	118.4	54.2
Modified R5: Leiner	215.7	68.3

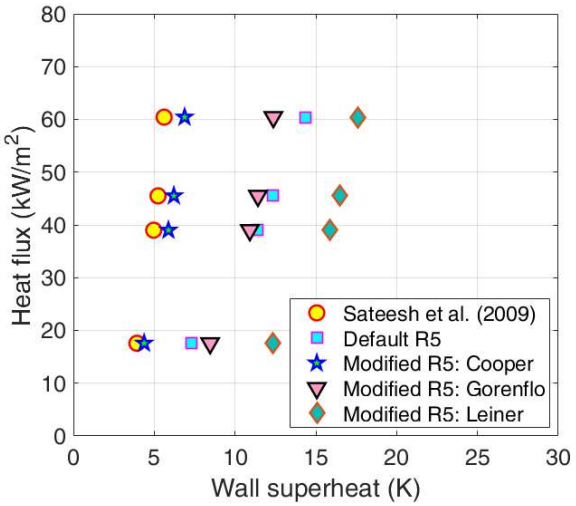

Figure 1. Nucleate pool boiling: q'' vs. ΔT_w

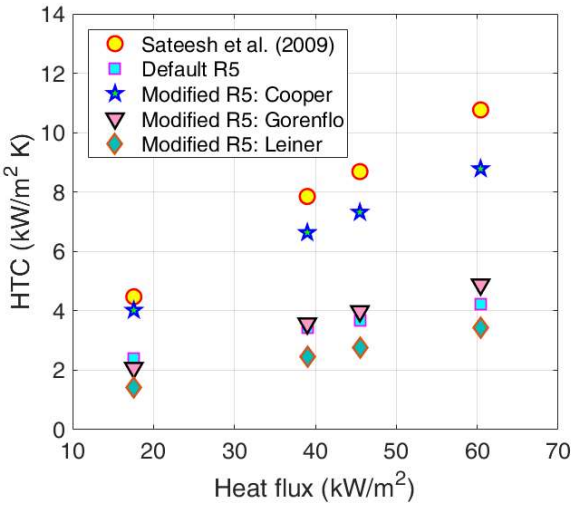

Figure 2. Nucleate pool boiling: HTC vs. q''

3.1.2 Film condensation in vertical tubes

Film condensation was extensively studied in the past. However, for geometries and conditions such as large tube diameter and high pressure, only few experimental data are available in literature. Among the campaigns described in section 2.2, the experiments performed by Kuhn et al. (1997) are selected for the V&V process of the modified R5. Despite this campaign was performed at low steam pressure, it represents the only available data on pure steam condensation in vertical tubes characterized by relatively large diameter. Kim and No (2000) performed specific tests investigating steam condensation in conditions relevant for passive safety systems, but these experiments do not agree with the scope of the present work for two reasons. In the first instance, the experimental campaign does not investigate the separate effect since the condensing pipe is submerged in a water pool. Several experiments, including Kuhn's tests, were led with a cooling jacket that allows a more accurate evaluation of the heat transfer and, thus, of the HTC. The second reason is that information about the mixture flow rate is not provided by Kim and No (2000). This parameter constitutes an

Annals of Nuclear Energy 160 (2021) 108436
https://doi.org/10.1016/j.anucene.2021.108436

essential boundary condition for the HTC evaluation, since film condensation heat transfer is strongly affected by the fluid velocity.

The experimental facility selected for the V&V process is described in detail Kuhn et al. (1997). The apparatus is composed of the instrumented test section, the steam and gas suppliers, a separator, a quench tank, and their connections. The test section consists of a condensing tube surrounded by a cooling jacket. Steam enters at the top of the inner tube, moving downward. Cooling water enters at the bottom of the annular region and it flows upward removing heat from steam. The condensing tube is made of 304 stainless steel and it has outer diameter of 50.8 mm. It is 3.37 m long, but the active length is limited to the lower 2.418 m. The adiabatic inlet ensures the reduction of entrance effects. Several thermocouples are installed within the annular region, measuring the temperatures of the inner and outer walls at different elevations. Kuhn et al. applied turbulent convective heat transfer theory to calculate bulk temperature. Such a methodology allows to reduce flow disturbance caused by instrumentation. In addition, cooling water bulk temperature is measured by TCs mounted at the inlet and outlet pipes and a movable thermocouple probe is installed to acquire vapor center-line temperature at different axial levels (Kuhn et al., 1997). The experimental uncertainties are reported by Shumway (1995). Uncertainty related to the temperature measurement at the inlet of the test section is evaluated equal to ±0.99 K and heat flux uncertainty is ±10.4 %. No information is provided for the wall temperature uncertainty.

The thermal-hydraulic modelling is limited to the test section. The condensing side comprehends a vertically oriented pipe component composed of 35 CVs for an overall length of 3.37 m. The upper part, not involved in the heat exchange, is modelled with a coarser mesh (five CVs 0.1904 m long), whereas the active length is characterized by a more detailed nodalization (thirty CVs 0.0806 long). This difference aims only to ensure a high resolution in the active region, since a sensitivity analysis demonstrated the independence of the results by axial meshing. Flow area and hydraulic diameter are imposed according to actual features of the apparatus. At the extremities, the pipe is connected with two branch components, through which inlet and outlet conditions are established. Boundary conditions are set with two time-dependent volumes, imposing steam inlet conditions and outlet pressure, and a time-dependent junction, which defines the total descending mass flow rate. The secondary side is modelled with an additional vertically oriented pipe component, adopting analogous nodalization scheme of the previous one. Flow area and hydraulic diameter are evaluated based on actual geometry. The ascending flow rate, the inlet temperature and the outlet pressure of the cooling water are fixed as boundary conditions. An overall number of 30 heat structures couples the lower part of the two pipe components for a total length of 2.418 m. Cylindrical geometry is considered, employing actual inner and outer radii of the condensing tube. Each heat structure is characterized by an active length of 0.0806 m. The modelling approach consists to simulate the secondary side as well, since Dittus and Boelter correlation (Eq. (3)) was extensively proven to guarantee an accurate estimation of the single-phase forced convection heat transfer. This methodology allows to avoid assumptions on the heat flux that could influence the results of the simulation (e.g., the axial position of the completed condensation, if it occurs).

Several experiments have been modelled, nevertheless only a single test case is presented. The other calculations present analogous outcomes discussed in the following. The selected test is called Run 1.1-5R1. It is the most comprehensive study available in the literature and, for this reason, it is chosen for the analysis. This run was performed at a pressure of 0.5 MPa. Steam and cooling water flow rates are respectively 61.3 and 1074.0 kg/hr. Cooling water enters the test section at 306.65 K.

Run 1.1-5R1 was performed at the higher pressure among the test matrix and thus at the higher temperature difference between primary and secondary sides. It determines the complete steam condensation, as can be

Annals of Nuclear Energy 160 (2021) 108436
https://doi.org/10.1016/j.anucene.2021.108436

noticed in Figure 3; here the mixture temperature T_m acquired by the movable TC probe and the outside wall temperature of the inner tube T_w are reported, versus the axial position. In Figure 3 and Figure 4 position 0 m coincides with the upper extremity of the active length and it increases in the descending direction. The position of complete condensation is clearly highlighted by the T_m and confirmed by the wall temperature. It is located at around 1.6 m, where a sharp change in the trend occurs. Both the codes provide a satisfactory prediction of the temperatures in the first 1.6 m. The good evaluation of the T_w proves the accuracy of the Dittus and Boelter application on the secondary side. Downward the 1.6 m, the modified R5 matches very well the experimental data, highlighting that the improved code is able to predict the correct position of the complete condensation and thus an effective evaluation of the steam condensation heat transfer. On the other hand, the calculation carried out with the default version of R5 shows the complete condensation downstream the experimental result, at about 2 m. It could be explained by the underrate of the condensation heat transfer coefficient. Figure 4 pictures the comparison of the heat flux. Concerning the experiment, only data upstream the complete condensation were used to evaluate the heat flux. The plot confirms the heat transfer underestimate of the default R5. Although the modified version of the code overestimates the heat flux over the whole condensing length, the discrepancy with experimental data is sufficiently reduced to a value lower than the experimental uncertainty. The accuracy of the evaluation is also demonstrated by the correct prediction of the complete condensation position. Downstream, the heat flux sharply decreases since single-phase forced convection is a worse heat transfer mode. Laminar wavy condensation prevails for most of the active length, as also confirmed by the boundaries range proposed by Shah (Eq. (12) and Eq. (13)). Close to the inlet of the active length, laminar condensation is predominant as is shown by the sharp change of the heat flux in the first three CVs of the simulations. This phenomenon is not detected by the experiment since TCs are not installed very close to the cooling jacket outlet.

The measured data versus the predicted quantities at the same axial position have been processed to obtain the RMSRE, using Eq. (16). The results are summarized in Table 2 and compared with available experimental uncertainties.

Table 2. Film condensation: summary of measurement uncertainties and calculated RMSRE (%)

	T_w	T_m	q''
Measurement uncertainty	N/A[1]	0.99 (K)[2]	10.4
Default R5	19.2	15.7	10.7
Modified R5	5.8	3.6	7.9

[1] Not available; [2] Absolute error

Annals of Nuclear Energy 160 (2021) 108436
https://doi.org/10.1016/j.anucene.2021.108436

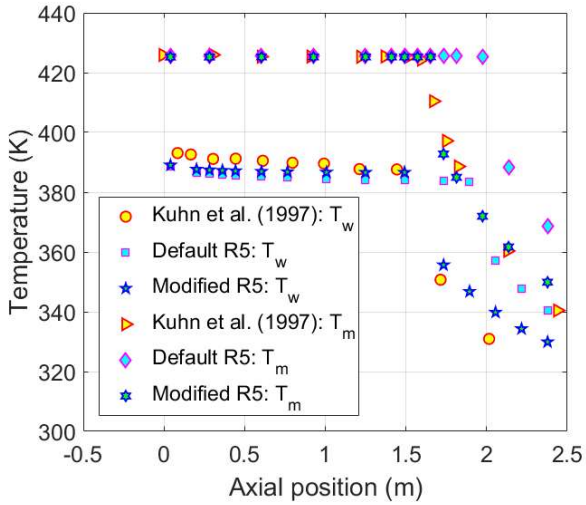

Figure 3. Film condensation: T vs. length

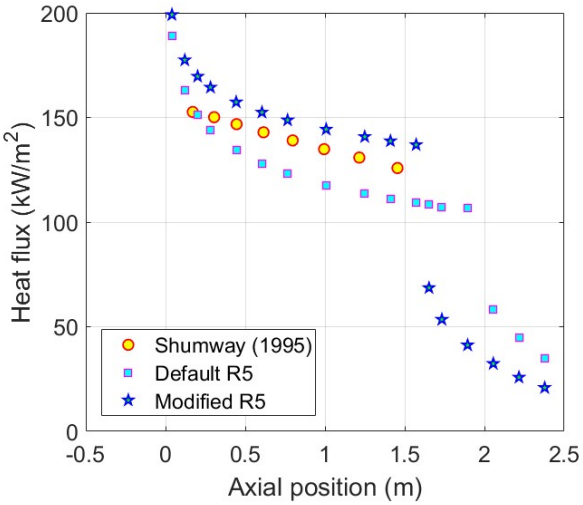

Figure 4. Film condensation: q'' vs. length

3.2 Integral effect validation

3.2.1 PERSEO experimental facility and selected test case

PERSEO is a full-scale facility built at SIET laboratories in Piacenza (Italy). The test section was designed in collaboration with ENEA to study an innovative passive emergency cooling system consisting of an isolation condenser submerged in a water pool at atmospheric conditions. The facility has a maximum power of around 20 MW and can operate up to BWR (or PWR secondary system) operative conditions.

The layout of the facility is fully described by Ferri et al. (2005). Figure 5 shows a schematic view of the main components. The primary system basically consists of the Pressure Vessel (PV), the HX and their connections. The PV is fed by steam from an external dedicated power station, which set thermodynamic conditions of the system. The isolation condenser is composed of two cylindrical headers and 120 vertical tubes that are 1.8 m in length and with outside diameter of 50.8 mm (non-dimensional length around 35). The secondary side comprehends two pools with different water inventory. The smaller one, referred as Heat eXchanger Pool (HXP), hosts the HX, whereas the larger one, the so-called Overall Pool (OP), operates as a water reservoir. The two pools are connected at the top with a steam duct and at the bottom with a water pipeline, equipped with a triggering valve.

In stand-by conditions, the HXP is empty, limiting heat exchange between HX and pool (see Figure 5a). The passive system is actuated opening the triggering valve: water flows by gravity from the reservoir to the HXP, flooding the isolation condenser (Figure 5b). The steam produced within the HXP moves through the steam duct. A conical shaped injector contributes to mix the steam with the residual water of the OP, performing the direct condensation and the partial restoration of the reserve. On the primary side, steam condenses within the tubes, enhancing the natural circulation through the primary loop (Ferri et al., 2005).

The facility is provided with a set of instruments for conventional thermal-hydraulic measures. Direct measurements (e.g. pressure, differential pressure, and temperature), are used to detect derived quantities (e.g. level, flow rate and heat exchange). Accuracy of the instruments was provided to the participants of the benchmark: accuracy of pressure transmitters is ±0.25% of the instrument full scale and nominal accuracy of the TCs is ±1.5 K. Moreover, Ferri et al. provide the estimated error of some derivative quantities: uncertainty

Annals of Nuclear Energy 160 (2021) 108436
https://doi.org/10.1016/j.anucene.2021.108436

of the level is ±0.04 m and accuracy of the HX heat exchange is ±500 kW (Ferri et al., 2005). The uncertainty related to the flow rate measurement is estimated to ±0.5 kg/s (Narcisi et al., 2020b).

The integral validation process has regarded the TEST 7. Nevertheless, only TEST 7 Part 1 is presented in this paper since analogous outcomes have been recognized from the simulation of Test 7 Part 2. The Part 1 is a full pressure test (7 MPa) aimed to analyse different operative conditions, assuming two water levels within the HXP: 1.4 m and 3.5 m (see Figure 5). The run starts in stand-by condition (Figure 5a). The test is divided in two opening phases of the triggering valve. During the first one the HXP level is increased up to 1.4 m, flooding the lower header and the final portion of the tubes. In the second phase the level grows up to 3.5 m, flooding the whole HX (Figure 5b). Three Phenomenological Windows (PhWs) are identified and summarized in Table 3.

Table 3. Phenomenological windows

PhW	Boundary Time (s)	Description
1	0-1260	HXP level increase in two phases and consequent heat transfer increase
2	1260-1845	Quasi-steady state operation with HXP level of 3.5 m
3	1845-4784	Boil-off and consequent level reduction and heat transfer decrease

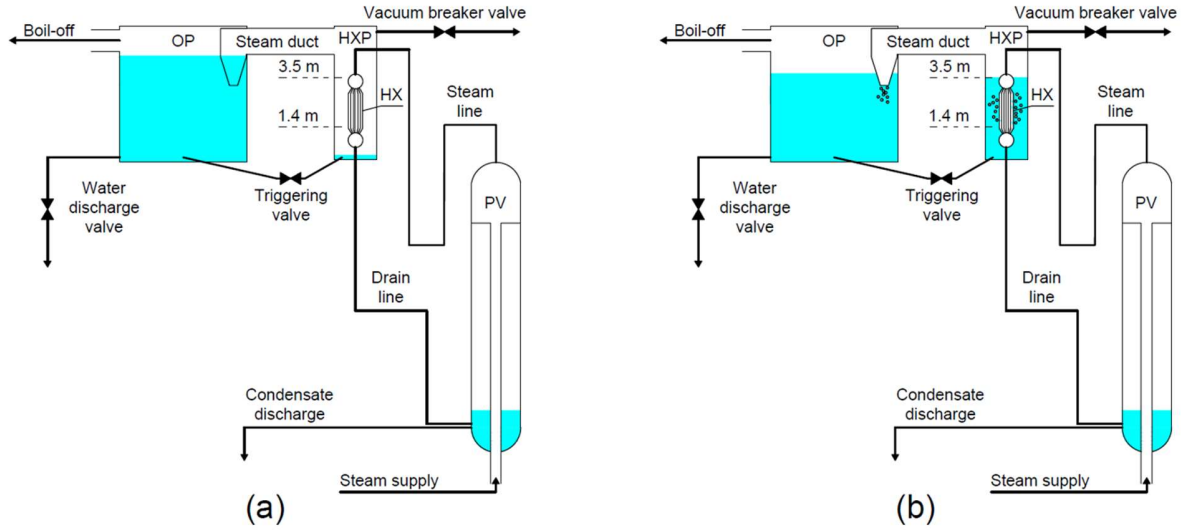

Figure 5. PERSEO layout: stand-by mode (a), operation mode (b)

3.2.2 Description of the thermal-hydraulic model

The thermal-hydraulic model was developed at DIAEE of "Sapienza" University of Rome (Narcisi et al., 2020b) for the validation benchmark promoted within the OECD/NEA/CSNI/WGAMA "Thermal-hydraulics of passive safety systems in water-cooled reactors" (Mascari et al., 2020).

The nodalization scheme is presented in Figure 6. It is partitioned in the primary and secondary system (respectively in orange - right side - and blue - left side - in Figure 6). The PV model consists of three "pipe" components. Two parallel pipes reproduce the main body of the PV, simulating the inlet steam conduit and the annular region between the duct and the PV's wall. The third one simulates the PV upper head. The HX's headers are modelled with two vertical pipes, each one composed of six CVs, and the tube bundle is collapsed in a single equivalent pipe component. Surface roughness is recognized to be an important parameter for an

Annals of Nuclear Energy 160 (2021) 108436
https://doi.org/10.1016/j.anucene.2021.108436

accurate estimation of the boiling heat transfer. However, information on this feature is not provided and the authors assume the value of 5 μm, typical for such applications.

Steam and drain lines, modelled with five pipes, connect HX and PV. Steam conditions are fixed by the time-dependent volume at the bottom of the PV's steam conduit. A further time-dependent volume, connected at the PV bottom, operates as a condensate drain system.

Each pool is simulated with two parallel pipes. For each tank, cross junctions join the CVs at the same level to reproduce buoyancy within the large volumes. A pipe component connects the two pools, simulating the steam duct and the injector. At the bottom, two pipes and a motor valve component model the water line and the triggering valve. Atmospheric conditions are fixed at the top of the reservoir with a time-dependent volume. In addition, a time-dependent volume is connected at the bottom of the OP, modelling the water discharge system (see also Figure 5). The HXP model is equipped with two time-dependent volumes connected to the pool with trip valve components: the first one set initial conditions for the test and the second one acts as vacuum breaker system (see also Figure 5).

The whole input is conceived with the slice modelling approach, with a refined mesh in the main heat transfer region.

An overall number of 74 heat structures fulfil the thermal coupling between primary system and HXP, including headers, tube bundle and the portion of steam and drain lines included within the HXP. Furthermore, several heat structures model the heat losses towards the environment, defined as a boundary condition in terms of outside temperature (288 K) and HTC (6 W/m^2 K).

The nodalization scheme presented in this section is the result of a mesh sensitivity analysis, performed to test the impact of different modelling methodologies on the simulation outcomes. The sensitivity analysis involved the main heat transfer regions, i.e., the pools and the heat exchanger.

As regard the pool modelling, two different approaches were assessed: a one-dimensional method, based on a single pipe component, and a "pseudo" multi-dimensional approach, based on multiple parallel pipes. The one-dimensional modelling represents the simplest solution, but simulation outcomes highlighted the limits of this approach. As matter of fact, the single pipe suppresses the buoyancy within the HXP, and thus prevents the wetting of the HX portion subjected to the highest heat flux. On the primary side, steam enters HX tubes from the upper boundary, leading to a strong condensation rate in the first portion of the tubes. In the single channel modelling, the absence of buoyancy within the HXP, causes the change of the heat transfer mode from nucleate boiling to transition boiling, above the half tubes length, and to film boiling at the very top of the tubes. In these conditions, despite the improvements implemented in the new version, the code experienced a significant underestimation of the total heat transfer, and thus the under prediction of the natural circulation in the primary loop. The inconsistency of the results was solved with a multiple channel modelling, consisting in the adoption of multiple parallel channels connected with several cross junctions. This approach guarantees the establishment of buoyancy and the wetting of the HX surfaces. In this case the nucleate boiling heat transfer mode is experienced on the total length of the HX tubes, resulting in a satisfactory agreement with experiment (see section 3.2.3). The influence of the number of parallel pipes was assessed, simulating the pools with two and three parallel components. The increase of the components number did not lead to noticeable improvements of the simulation outcomes, therefore the higher computational costs is not worth.

Concerning the axial discretization of the most relevant heat transfer region, the consequence of reducing the average CV's length was assessed. This parameter was assumed equal to 187 mm and 93.5 mm. Both the

Annals of Nuclear Energy 160 (2021) 108436
https://doi.org/10.1016/j.anucene.2021.108436

simulations provided a satisfactory agreement with experimental data, succeeding in the reproduction of the most significant phenomena. However, reducing the average meshing of the heat transfer region allowed to reduce the stepwise trend observed in the heat transfer and primary flow coast-down. Indeed, as the level within the HXP decreases, the HX tubes are progressively uncovered, and the discretization assumed in the modelling causes the typical stepwise trend. It was proven that such behaviour can be limited by reducing the axial length of the computational nodes. Therefore, in the final model, an average length of 190 mm is adopted, except for the pools and the HX where an average meshing of 90 mm is adopted.

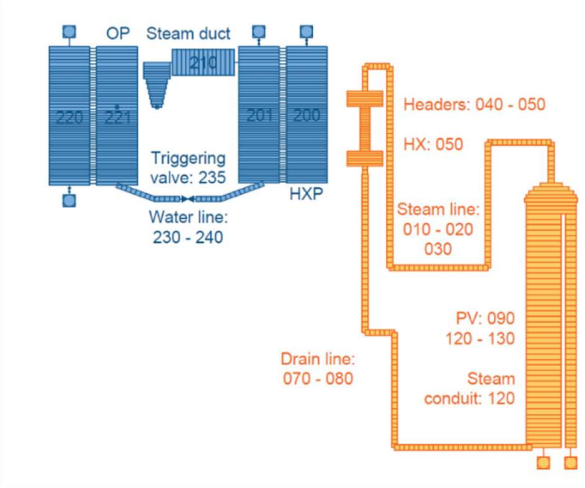

Figure 6. PERSEO thermal-hydraulic model

3.2.3 Results and discussion

In this section, simulation results, obtained with the default and the modified R5, are compared with the experimental data, highlighting the improvements of the modified version of the code. A time step sensitivity has been preliminary carried out to evaluate the effect of such parameter on the simulation outcomes. The time step has been progressively reduced from the highest value of 5.0×10^{-3} s to the lowest 5.0×10^{-4} s. The analysis has demonstrated the independence of the results by the time step and thus the highest value has been assumed for the present activity. All the observed thermal-hydraulic parameters present visible fluctuations, that are not suppressed if the time step is lowered. The oscillations are magnified with the modified version of the code, although the verification process has not highlighted such behavior. The explanation could be derived from the experimental acquisition, that experienced similar oscillatory trends. Even if there is not an evidence, such fluctuations seem to be related to the two-phase operative conditions. This could justify the larger fluctuations observed in the modified version of the code, that predicts higher boiling and condensing rates than the default R5.

Initial conditions supplied to the participants of the validation benchmark are used for the present activity. The initial primary flow rate is imposed to 0 and saturated conditions are set in the primary system. The pressure of the secondary system is imposed to 0.1 MPa and the starting free level is set to 0.19 m in the HXP and to 4.65 m in the Overall Pool (OP, level 0 coincides with the OP bottom).

In the following plots, both code versions outcomes are compared with experimental data. The three PhWs are distinguished with the vertical dashed lines. The duration of the second PhW is a relevant parameter for the assessment of the simulation accuracy. In this time frame occurs the quasi-steady state operation with HXP level at 3.5 m, that is strongly affected by the HX heat transfer. As matter of fact, heat exchange undervalue

Annals of Nuclear Energy 160 (2021) 108436
https://doi.org/10.1016/j.anucene.2021.108436

yields a slower water consumption within the HXP and, thus, the persisting of the quasi-steady state conditions.

Figure 7 shows the HXP and OP free level. Initial steady state conditions are kept up to 475 s, when the first opening of the triggering valve is commanded. In this phase, a low primary mass flow rate is detected by the instrumentation (see Figure 8). It should be noted that, in this time lapse, the presence of air within the HXP limits the HX heat transfer. It means that, in the first 475 s, the primary flow rate is promoted by the heat losses. Although calculations start with null mass flow rate, it quickly increases to 0.78 kg/s in both the simulations. In fact, modifications introduced in R5 do not interfere in the first phase of the test. Nevertheless, the discrepancy with the experiment is limited to 0.3 kg/s, i.e., lesser than the experimental uncertainty. It should be noted that, at very low flow rates, the accuracy of the instrument is expected to be lower than the value declared.

Figure 9 shows the heat exchange between HX and HXP. At the beginning of the test, the numerical predictions poorly match experimental data. The large difference, observed over the whole test, is explained keeping in mind the experimental evaluation of the heat transfer. This value is obtained by the relation expressed in Eq. (17):

$$Q = \Gamma\left(H_g - H_f\right) \tag{17}$$

where Γ is the mass flow rate, H the specific enthalpy evaluated at the measured temperature and pressure, and the subscripts g and f stand respectively for steam and liquid phases. It is supposed that all the steam entering the HX condenses and, consequently, saturated liquid water exits the IC and flows back to the PV. Nevertheless, there is no evidence that the total steam flow rate is condensed, even more at the beginning of the test, when the HXP is empty. This justifies the large discrepancy observed in Figure 9.

Before the actuation of the system, the HXP relative pressure is controlled to agree with the experimental data (around 0.6 kPa, see Figure 10). Figure 11 depicts the differential pressure through the injector. The value acquired in the first 475 s is related to the gravity head of the liquid water contained within the injector (see Figure 5a for a picture of the stand-by conditions). The outside wall temperature of the tube bundle is shown in Figure 12. The experimental acquisition is obtained by five TCs installed at the top of the bundle, on five different tubes. The measurements are compared with the average outside wall temperature calculated at the same vertical position. As expected, before the operation of the system, equilibrium conditions are well predicted so that the wall temperature approaches the saturated temperature at 7 MPa.

Following the first opening of the triggering valve, water streams from the reservoir towards the HXP by gravity. The free level within the HXP grows up to around 1.4 m, flooding the lower header and the bottom part of the tubes. Figure 7 shows a satisfactory detection of the level change within OP and HXP. The safety system is partially actuated, and a limited portion of the steam starts to condensate within the HX lower header, promoting the primary flow rate increase up to 2 kg/s. In this phase, the improvements of the modified R5 plays a crucial role. The stronger heat transfer (see Figure 9) results in a higher primary flow rate and discrepancy with experimental data is significantly reduced (Figure 8). A large difference in terms of HX power is still present, however, and it is explained by Eq. (17).

Flow rate between the two pools is regulated by the pressure reached at the top of the HXP. As water enters, boiling occurs, and the steam produced pressurized the HXP, limiting the inlet flow rate. Focusing on the simulations, after the opening of the triggering valve, the trip valve component, that sets initial conditions within the HXP, closes. This determines the quick increase of the HXP pressure, in accordance with the experimental data. The HXP relative pressure reaches the value of 12.5 kPa (Figure 10) that is enough to push

Annals of Nuclear Energy 160 (2021) 108436
https://doi.org/10.1016/j.anucene.2021.108436

water out of the injector. Thus, the gravity head within the injector is suppressed and differential pressure through this component assumes a null value (Figure 11).

The abovementioned conditions are kept up to 1039 s, when the second opening of the triggering valve is actuated. The maximum value of the HXP level occurs at 1260 s, when the second PhW starts. The maximum value of 3.5 m is well predicted by the modified R5, in terms of magnitude and time lapse. On the other hand, the default R5 predicts a higher maximum level, delayed of about 170 s (Figure 7). Following the second opening of the triggering valve, the instruments detect a decrease of the HXP pressure: at first negative spikes are observed (restored by the vacuum breaker system) and then the prolonged pressure reduction is measured, reaching the minimum value of 8.5 kPa at 1260 s. It is explained by the partial condensation induced within the HXP by the cold water coming from the OP. Both the simulations do not detect the pressure negative spikes, still the prolonged pressure decrease is narrowly simulated (Figure 10). In the default R5 calculation, the minimum pressure is kept up to 1430 s, inducing the delay of the maximum HXP level.

As the HX is flooded, heat exchange increases due to the more efficient heat transfer mode (the nucleate boiling). The first peak value is reached at 1214 s. At this time step, the enhanced capabilities of the modified R5 are magnified. The improved version of the code calculates a peak of 17.2 MW compared to the 12.4 MW of the default R5. A discrepancy with experiment is still observed, even if it is subjectable to the experimental methodology for derivation of the heat transfer starting from the mass flow rate and based on the assumption of complete condensation. The accuracy of the modified R5 simulation is demonstrated in Figure 8. The increase in the primary flow rate approaches very well the experimental data. The first peak of around 12 kg/s is reached at 1260 s. At this time, the default version of the code simulates a peak substantially lower (about 7 kg/s), in accordance with the heat transfer underestimate. The heat transfer rise is temporarily interrupted by the prolonged pressure decrease within the HXP. At the beginning of the second PhW, the HX is almost completely flooded, and the boiling rate reaches the maximum value. This condition leads to the quick increase of the HXP pressure. The default R5 underestimates this phenomenon. The maximum value is delayed (Figure 10), explaining the discrepancies observed in the HXP maximum level. On the other hand, the improved version of the code provides a reasonable agreement with the experimental pressure increase. Although the prompt pressure rise is overestimated, the maximum value obtained at 1845 s approaches properly the experimental peak, leading to the accurate reproduction of the HXP level increase.

At 1530 s, the maximum power is reached. Quasi-steady state conditions are observed up to 1845 s. The accuracy in predicting the second PhW duration confirms the solidity of the modified R5. Figure 8 and Figure 9 shows a satisfactory match between experiment and enhanced R5 calculation, in terms of time frame of the quasi-steady state operation. A sensitivity analysis on the surface roughness of the tubes has shown the negligible effect of this parameter on the system operation. Roughness has been changed in the range of 7.5-2.5 μm and compared with the reference calculation. The maximum deviation of the quasi-steady state power is recognized to be 0.9 %. No significant effects are observed for primary flow rate and for the time lapse of the second PhW.

Concerning the simulation performed with the default code, the duration of the quasi-steady state is over predicted, due to the lower water consumption within the HXP. Indeed, the HXP level decreases slower than the experimental one. In quasi-steady state conditions, the primary flow rate discrepancy decreases from 41% (default R5) to 4.5% (modified R5). The steam produced within the HXP flows towards the OP, moving through the steam duct. Differential pressure through the injector rises to 10 kPa, due to the pressure drop induced by the steam flow rate. Figure 11 highlights a good agreement between experiment and improved R5, proving the correct estimation of the steam flow rate. Focusing on the boiling heat transfer, the outer wall temperature of

Annals of Nuclear Energy 160 (2021) 108436
https://doi.org/10.1016/j.anucene.2021.108436

the HX tubes provides an assessment of the simulation accuracy. Unless the fluctuations (typical of two-phase problems), the modified version of the code shows a good match with the experiment during the quasi-steady state operation (Figure 12). On the other hand, the default calculation yields a visible over prediction of the wall temperature (around 40 K), confirming the undervalue of the heat transfer (in both boiling and condensing modes). Information on tube side is not available and uncertainty related to the experimental calculation of the HX power makes difficult to extrapolate the condensing HTC. Nevertheless, a graphic representation of the calculated HTC along the HX tube, comparing results of the default and the modified versions of the code, can help the quantification of such underestimation. Figure 13 shows the HTC computed by the two versions of the code for each HX heat structure at 1700 s (quasi-steady state operation, second PhW). In addition, the flow regime evaluated at the same time in each CV is presented in Figure 14. For these two plots, the upper boundary of the HX tubes (i.e., primary steam inlet) is selected as reference level (x = 0 in figures) and the length increases descending towards the bottom outlet of the tubes. Figure 13 shows that the highest improvement in terms of HTC is experienced on the pool side, where the modified R5 calculates a coefficient one order of magnitude higher than default code. Focusing on the condensation heat transfer, the modified version of the code obtains an HTC almost two times higher than default R5. This is due to the different heat transfer mode predicted by the codes: laminar (lam in Figure 14) condensation for default R5 and wavy laminar (wlam in Figure 14, note that this flow regime has been implemented in the improved R5) condensation in the modified code. It is worth noticing that default R5 computes the same order of magnitude for pool boiling and condensation HTCs, especially at the HX top where higher heat flux is experienced. The difference increases along the tube length, reaching the maximum at the HX bottom where pool boiling HTC results two times the condensation coefficient. This means that, especially at the top of the HX, the thermal resistance evaluated by the default R5 is comparable in the two sides of the heat exchanger. On the other hand, the modified version of the code experiences a relevant improvement of the pool boiling HTC, leading to a minor contribution to the overall thermal resistance. Regarding the flow regime, both the codes predict subcooled nucleate boiling (sub-b in Figure 14) at the bottom and saturated nucleate boiling (sat-b in Figure 14) at the top of the HXP. The difference between the two versions of the code is observed in the level of the transition from sub-b to sat-b. More specifically, due to the higher heat flux estimated by the modified R5, this version of the code predicts such transition around 0.3 m below the prediction of default R5.

The third PhW is characterized by the boil-off and the consequent HXP level decrease. The triggering valve is closed and the water consumption within the HXP leads to the progressive uncovering of the HX. Figure 7 shows a fair accordance between experimental data and modified R5 results in terms of level reduction. The reasonable match is also observed for the primary flow rate and the HX power. The miscalculation of the boiling rate provided by the default R5 leads to the delay of HX uncovering and to the consequent slower flow rate and power decrease. The uncovering of the TCs leads to the quick temperature increase shown in Figure 12, explaining the delay observed in the default R5 simulation. Wall temperature is acquired at different levels of the bundle. Nevertheless, only TCs acquisition at the top of the tubes is presented. The comparison between experiment and simulations confirms the same outcomes over the whole length of the tube bundle.

As the boiling rate decreases, the relative pressure within the HXP reduces (Figure 10). Differential pressure through the injector progressively falls to 0, pushing the water free level outside the injector. It supports the final value of the HXP relative pressure, which coincides with the gravity head associated to the level difference between the injector and the OP.

Annals of Nuclear Energy 160 (2021) 108436
https://doi.org/10.1016/j.anucene.2021.108436

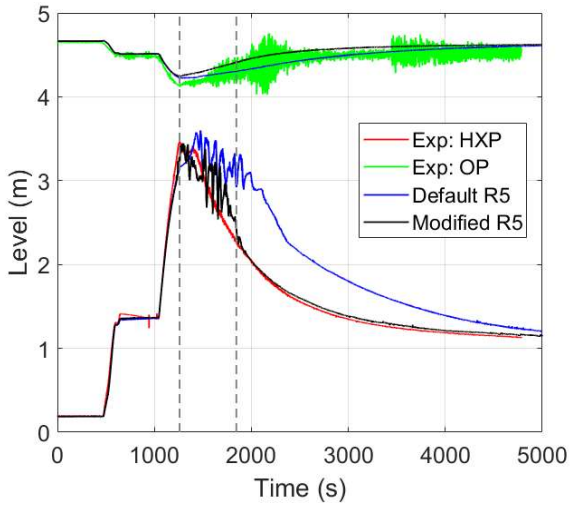

Figure 7. HXP and OP levels

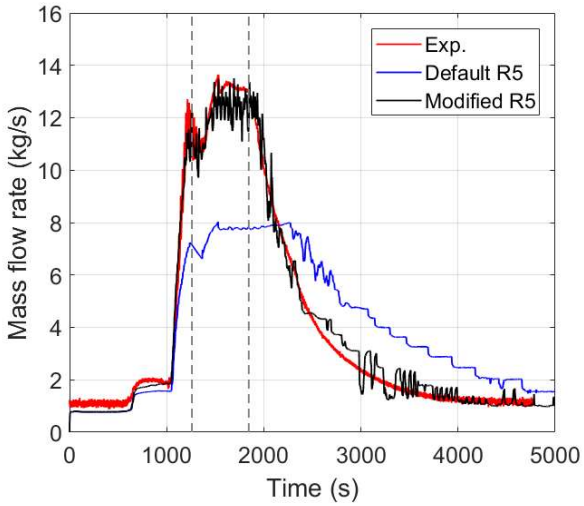

Figure 8. Primary mass flow rate

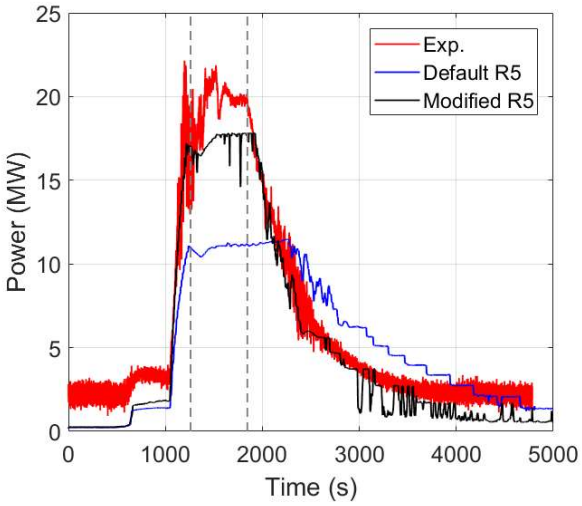

Figure 9. HX power

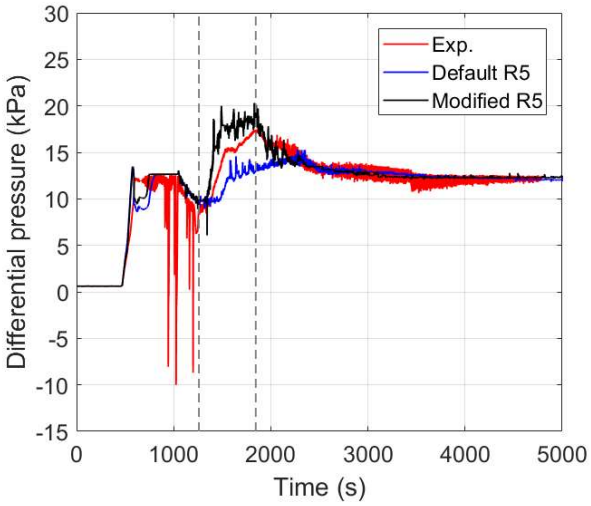

Figure 10. HXP relative pressure

Annals of Nuclear Energy 160 (2021) 108436
https://doi.org/10.1016/j.anucene.2021.108436

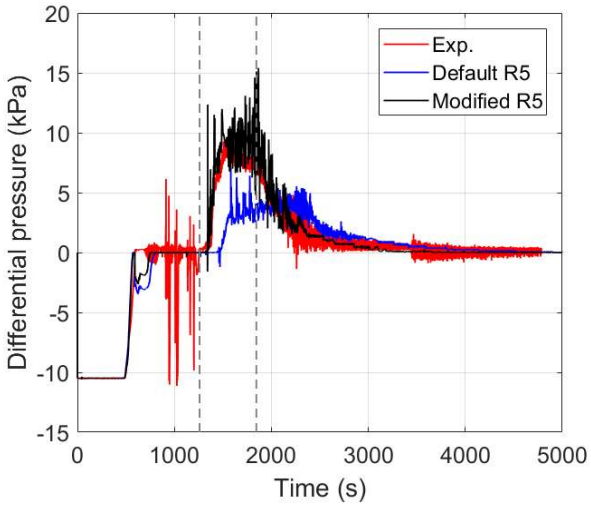

Figure 11. Injector differential pressure

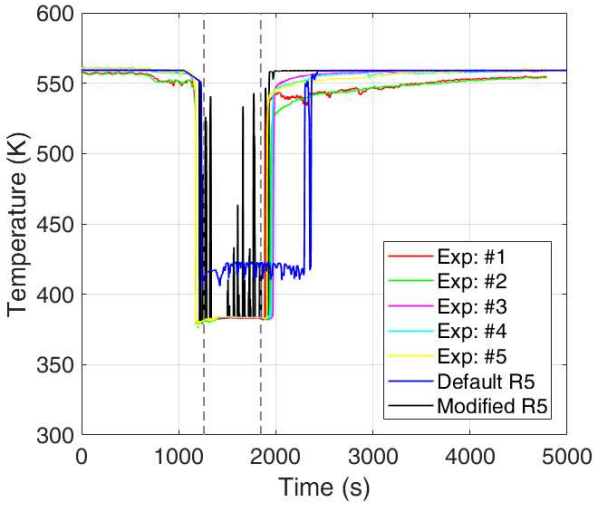

Figure 12. Tube bundle outside wall temperature

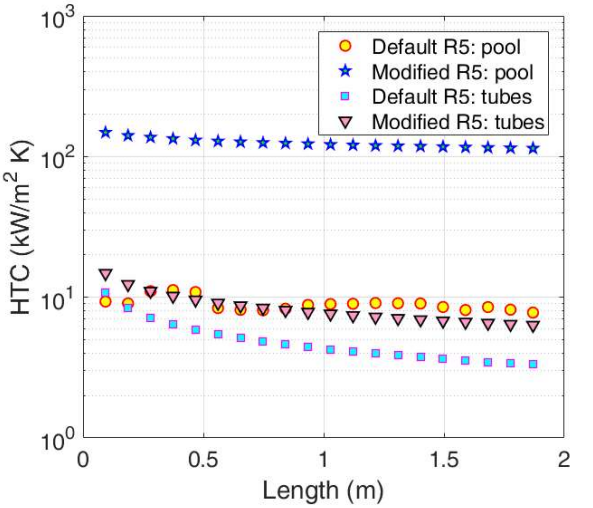

Figure 13. PhW 2 (1700 s): HTC vs. HX tube length (simulations only)

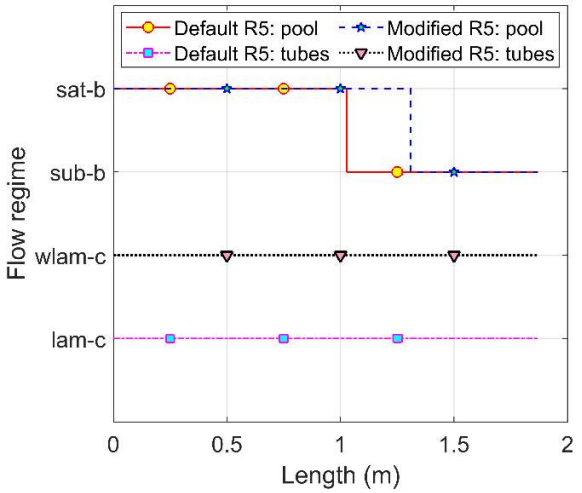

Figure 14. PhW 2 (1700 s): Flow regime vs. HX tube length (simulations only)

4 Conclusions and perspectives

In the past, several activities showcased limited capability of system thermal-hydraulic codes to properly model heat transfer phenomena within in-pool passive power removal system. Some works involved PERSEO facility in assessing the predictions of the most used BE codes, such as RELAP5, TRACE and CATHARE. More recently the same experimental data were used in a benchmark exercise proposed within the OECD/NEA/CSNI/WGAMA "Thermal-hydraulics of passive safety systems in water-cooled reactors". The most relevant issue, observed in each different activity, was the significant underestimate of the heat transfer in a passive removal system comprehensive of an in-pool heat exchanger. Researchers related the significant underprediction of the heat exchange to the HTC evaluation, considering that the correlations employed for the coefficient computation are not suitable for the passive system operative conditions.

Annals of Nuclear Energy 160 (2021) 108436
https://doi.org/10.1016/j.anucene.2021.108436

Nowadays, the most widespread approach is to optimize heat transfer analysis by tuning HTC with calibrated multiplicative factors. Although this methodology is proven to give satisfactory results, it is not ideal for best estimate calculations since the enhancing factors depend on many parameters that cannot be quantified a priori. Moreover, despite simulating the same experiment, researchers proposed different solutions to overcome the abovementioned issue, demonstrating the complex nature of the problem.

With the purpose to make a numerical tool able to handle heat transfer phenomena occurring in such passive safety systems, DIAEE of "Sapienza" University of Rome has started a developing activity on the RELAP5/Mod3.3 code. State of the art has been extensively studied and summarized in this paper. The proposed modifications have involved two heat transfer mechanism: the nucleate boiling and the film condensation. The default version of the code lacks a specific boundary condition type for pool boiling, whereas the contribution of the nucleate boiling is evaluated by Forster and Zuber correlation, exploited in Chen's formulation of the HTC. In the modified R5, a new boundary condition type has been implemented, replacing the Chen equation with a more eligible correlation for pool boiling, formulated by Cooper. This correlation accounts for the effect of relevant parameters, such as surface roughness, operative pressure, and fluid properties. Dealing with the film condensation in vertical tubes, the original version of the code computes the HTC as the maximum of the Nusselt and Shah values. The set of correlations has been improved in the modified R5, including a more adequate correlation for HTC evaluation in laminar wavy condensation (Kutateldze) and updating the Shah correlation with the most recent formulation derived by the same author. These implementations aim to extend the applicability range of the code to low flow rates and high operative pressures cases.

The V&V process of the R5 improved version involved the single effect validation, by mean of simple test cases, as well as the integral effect analysis supported by experimental data from the PERSEO facility. The nucleate pool boiling assessment has been led comparing code outcomes with an experimental campaign performed by Sateesh et al. (2009), where a vertical cylindrical heater is submerged in a water pool at ambient conditions. The RMSRE of wall superheat is proven to be reduced from 1.290 to 0.182 using the modified version of the code. Concerning the film boiling, the improved set of correlations has been tested towards experimental data from the campaign performed by Kuhn et al. (1997). The facility consisted of a condensing vertical tube surrounded by a cooling jacket. The enhanced R5 shows relevant betterments in the evaluation of the complete condensation length. As matter of fact, RMSRE of the wall temperature is reduced from 0.192 to 0.058.

The integral effect assessment has relied on experimental data of Test 7 Part 1 performed in the PERSEO facility. This test investigates the behaviour of a full-scale in-pool heat exchanger at different water levels. The passive system is actuated by opening the triggering valve that connects the water reservoir with the HXP. Water flows by gravity, flooding the isolation condenser. Boiling amplifies the heat transfer, leading to steam condensation within the HX tubes that promotes natural circulation through the primary system. A qualitative comparison between the experimental data and the calculations highlights the significant enhancement of the simulation results adopting the modified code. The most relevant parameters (e.g., primary flow rate, water free level, HXP pressure, wall temperature) have been predicted with a reasonable agreement, proving the efficacy of the new implementations.

The code development discussed in this paper has drastically increased the prediction capability of R5 for simulation of advanced in-pool passive power removal systems. Nevertheless, the validation process needs to be extended to prove the applicability of the code to a wide range of safety-relevant situations. For what concerns the nucleate boiling, Cooper correlation was developed mainly for flat plates and horizontal cylinders

Annals of Nuclear Energy 160 (2021) 108436
https://doi.org/10.1016/j.anucene.2021.108436

and, albeit the correlation was validated for a wide range of reduced pressure and surface roughness, the combined effect of these two parameters was not exhaustively investigated. There is only one notable study, performed by Nishikawa et al. (1982), that includes the evaluation of the combined effect with a wide range of roughness but a modest range of pressure ($0.08<p_r<0.9$). The lack of dedicated studies and information is even greater for vertical cylinders. For this reason, future activities will be focused on the experimental investigation of nucleate pool boiling on vertical cylinders, enlarging available data set at low pressure and high roughness (R > 1 μm). For film condensation heat transfer, most of the available experimental data at low velocity are supplied at low pressures, typical of PCCS. Future works could be dedicated to the experimental analysis of film condensation at high pressures, up to BWR (or PWR secondary system) operative conditions. Further information will derive from the experimental facility SIRIO, designed as part of a collaboration started in 2017 between the Italian industries (SRS, ANSALDO and SIET) and ENEA to test the innovative safety system proposed for ALFRED (Alemberti et al., 2020; Marinari et al., 2018). It will also allow the assessment of code predictability for steam condensation with the presence of non-condensable gas.

The knowledge derived from these experimental investigations will cover some lack of experimental database allowing to widen the essential validation program.

Acknowledgements

The authors wish to thank Prof. Gianfranco Caruso, for the review and the valuable suggestions, and they would like to express their gratitude to ENEA for distributing the PERSEO facility and Test 7 description and the Test 7 experimental data along the OECD/NEA/CSNI/WGAMA activity on the “Status report on thermal-hydraulic passive systems design and safety assessment”.

Acronyms

AHWR	Advanced Heavy Water Reactor
ALFRED	Advanced Lead Fast Reactor European Demonstrator
APR+	Advanced Power Reactor Plus
BWR	Boiling Water Reactor
CAMP	Code Applications and Maintenance Program
CSNI	Committee on the Safety of Nuclear Installations
CV	Control Volume
DHR	Decay Heat Removal
DIAEE	Department of Astronautical, Electrical and Energy Engineering
ELAP	Extended Loss of AC Power
ENEA	Italian National Agency for New Technologies, Energy and Sustainable Economic Development
GEN-IV	Generation IV
HTC	Heat Transfer Coefficient
HX	Heat eXchanger
HXP	Heat eXchanger Pool
IAEA	International Atomic Energy Agency
IC	Isolation Condenser
ICAP	International Code Assessment and Application Program
iPOWER	Innovative Power Reactor
lam	Laminar

Annals of Nuclear Energy 160 (2021) 108436
https://doi.org/10.1016/j.anucene.2021.108436

LFR	Lead-cooled Fast Reactor
LWR	Light Water Reactor
N/A	Not available
NPP	Nuclear Power Plant
NRC	U.S. Nuclear Regulatory Commission
OECD/NEA	Organization for Economic Co-operation and Development – Nuclear Energy Agency
OP	Overall Pool
PCCS	Passive Containment Cooling System
PERSEO	in-Pool Energy Removal System for Emergency Operation
PhW	Phenomenological Window
PV	Pressure Vessel
PWR	Pressurized Water Reactor
R5	RELAP5/Mod3.3
R5-3D	RELAP5-3D©
RMSRE	Root Mean Squared Relative Error
sat-b	Saturated nucleate boiling
SBWR	Simplified Boiling Water Reactor
STH	System Thermal-Hydraulic
sub-b	Subcooled nucleate boiling
TC	Thermocouple
V&V	Verification and Validation
WGAMA	Working Group on the Analysis and Management of Accidents
wlam	Wavy laminar

Nomenclature

cp	Specific heat at constant pressure (J/kg K)
D	Inside tube diameter
D_H	Hydraulic diameter (m)
F	Reynolds number factor
G	Total mass flux (kg/m^2 s)
g	Acceleration of gravity
H	Specific Enthalpy (J/kg)
h	Heat transfer coefficient (W/m^2 K)
J	Dimensionless velocity
k	Thermal conductivity (W/m K)
M	Molecular weight
N	Number of observations
p	Pressure (Pa)
Pr	Prandtl number
Q	Heat exchange (W)
q''	Heat flux (W/m^2)
R	Roughness (µm)
$R_{p,old}$	"Glättungstiefe" according to DIN 4762/1:1960 (µm)
Re	Reynolds number
S	Suppression factor

T	Temperature (K)
x	Flow quality
y	Quantity
Z	Shah's correlating parameter

Greek symbols

Γ	Mass flow rate (kg/s)
δ	Film thickness (m)
λ	Thermal conductivity (W/m K)
Δ	Increment
μ	Dynamic viscosity (Pa/s)
ρ	Density (kg/m^3)
σ	Surface tension (N/m)

Subscripts

e	Experiment
f	Saturated liquid/liquid phase
g	Saturated vapor, vapor/gas phase
m	Mixture
nb	Nucleate boiling
Nu	Nusselt equation
r	Reduced
s	Simulation
sat	Saturated
sp	Single-phase
tp	Two-phase
w	Wall

References

Alemberti A., Caramello M., Frignani M., Grasso G., Merli F., Morresi G., Tarantino M., 2020. ALFRED reactor coolant system design. Nucl. Eng. Des. 370, 110884. https://doi.org/10.1016/j.nucengdes.2020.110884

Bae B.U., Yun B.J., Kim S., Kang K.H., 2012. Design of condensation heat exchanger for the PAFS (Passive Auxiliary Feedwater System) of APR+ (Advanced Power Reactor Plus). Ann. Nucl. Energy 46, 134-143. http://dx.doi.org/10.1016/j.anucene.2012.03.029

Annals of Nuclear Energy 160 (2021) 108436
https://doi.org/10.1016/j.anucene.2021.108436

Balestra P., Giannetti F., Caruso G., Alfonsi A., 2016. New RELAP5-3D lead and LBE thermophysical properties implementation for safety analysis of Gen IV reactors. Sci. Technol. Nucl. Ins. 2016. https://doi.org/10.1155/2016/1687946

Barone G., Martelli D., Forgione N., 2019. Implementation of Lead-Lithium as working fluid in RELAP5/Mod3.3. Fusion Eng. Des. 149 (Part A), 1308-1312. https://doi.org/10.1016/j.fusengdes.2019.02.064

Bersano A., Bertani C., Falcone N., De Salve M., 2020. Qualification of RELAP5-3D code against the in-pool passive energy removal system PERSEO data. In: Proceedings the 30th European Safety and Reliability Conference and the 15th Probabilistic Safety Assessment and Management Conference, Venice, Italy, November 1-5.

Bianchi F., Meloni P., Ferri R., Achilli A., 2004. Assessment of RELAP5 mod3.3 and CATHARE 2 v1.5A against a full scale test of PERSEO device. In: Proceedings of the 12th International Conference on Nuclear Engineering, Arlington, Virginia, USA, April 25-29.

Caramello M., Gregorini M., Bertani C., De Salve M., Alemberti A., Panella B., 2017. Thermal-hydraulic analysis of a passively controlled DHR system. Prog. Nucl. Eng. 99, 127-139. https://doi.org/10.1016/j.pnucene.2017.05.015

Challberg R.C., Cheung Y.K., Khorana S.S, Upton H.A., 1998. ESBWR evolution of passive features. In: Proceedings of the 6th International Conference on Nuclear Engineering, American Society of Mechanical Engineers, San Diego, USA.

Chen J.C., 1962. A correlation for boiling heat transfer to saturated fluids in convective flow. Brookhaven Natl. Lab., pp. 2-6. BNL-6672.

Chen W., Fang X., 2014. A note on the Chen correlations of saturated flow boiling heat transfer. Int. J. Refrig. 48, 100-104. https://doi.org/10.1016/j.ijrefrig.2014.09.008

Chen J.C., 1966. Correlation for boiling heat transfer to saturated fluids in convective flow. Ind. Eng. Chem. Process Des. Dev. 5 (3), 322-329. https://doi.org/10.1021/i260019a023

Chun M.H., Kang M.G., 1998. Effects of Heat Exchanger Tube Parameters on Nucleate Pool Boiling Heat Transfer. J. Heat Transf. 120 (2) 468-476. https://doi.org/10.1115/1.2824272

Cooper M.G., 1984. Heat Flow Rates in Saturated Nucleate Pool Boiling—A Wide-Ranging Examination Using Reduced Properties. Adv. Heat Tran. 16, 157-239. https://doi.org/10.1016/S0065-2717(08)70205-3

Dasgupta A., Chandraker D.K., Nayak A.K., Kulkarni P.P., Chinchole A., Rao R., 2017. Demonstration of adequacy of passive in-bundle ECC injection of AHWR. Ann. Nucl. Energy 102, 11-22. http://dx.doi.org/10.1016/j.anucene.2016.12.005

Dittus F.W., Boelter L.M.K., 1985. Heat transfer in automobile radiators of the tubular type. Int. Commun. Heat Mass 12 (1), 3-22. https://doi.org/10.1016/0735-1933(85)90003-X

Ferri R., Achilli A., Cattadori G., Bianchi F., Meloni P., 2005. Design, experiments and Relap5 code calculations for the Perseo facility. Nucl. Eng. Des. 235 (10-12) 1201-1214. https://doi.org/10.1016/j.nucengdes.2005.02.011

Forster H.K., Zuber N., 1955. Dynamics of vapor bubbles and boiling heat transfer. AIChE 1 (4), 531-535. https://doi.org/10.1002/aic.690010425

Foust O.J., 1972. Sodium-NaK engineering handbook. Volume I. Sodium chemistry and physical properties, Gordon and Breach, New York.

Giannetti F., D'Alessandro T., Ciurluini C., 2019. Development of a RELAP5 mod3.3 version for FUSION applications. DIAEE Sapienza University of Rome, pp. 1-51. D1902_ENBR_T01 Rev. 01.

Glaeser H., 2017. Verification and validation of system thermal-hydraulic computer codes, scaling and uncertainty evaluation of calculated code results, in: D'Auria F., 2017. Thermal-Hydraulics of Water Cooled Nuclear Reactors, first edition, Woodhead Publishing, Cambridge, pp 831-903.

Gorenflo D., 1993. Pool boiling, VDI Heat Atlas, VDI Verlag, Düsseldorf.

Guichet V., Jouhara H., 2020. Condensation, evaporation and boiling of falling films in wickless heat pipes (two-phase closed thermosyphons): A critical review of correlations. Int. J. Thermofluids 1-2 100001. https://doi.org/10.1016/j.ijft.2019.100001

Gupta A., Kumar R., Kumar V., 2010. Nucleate pool boiling heat transfer over a bundle of vertical tubes. Heat Mass Transfer 37 (2), 178-181. https://doi.org/10.1016/j.icheatmasstransfer.2009.06.023

IAEA, 2009. Safety Assessment for Facilities and Activities. Safety Standards Series No GSR Part 4 – General Safety Requirements. Vienna.

IAEA, 2016. IAEA Safety Glossary, Terminology Used in Nuclear Safety and Radiation Protection. Vienna, June.

Jain V., Nayak A.K., Dhiman M., Kulkarni P.P., Vijayan P.K., Vaze K.K., 2013. Role of passive safety features in prevention and mitigation of severe plant conditions in Indian Advanced Heavy Water Reactor. Nucl. Eng. Technol. 45 (5), 625-636. https://doi.org/10.5516/NET.03.2013.013

Jiang Y., Ren L., Zhikang L., Xi H., Ting W., 2017. Transient analysis of AP1000 NPP under the similar Fukushima accident conditions. Ann. Nucl. Energy 108, 181-187. http://dx.doi.org/10.1016/j.anucene.2017.04.026

Jones B.J., McHale J.P., Garimella S.V., 2009. The influence of Surface Roughness on Nucleate Pool Boiling Heat Transfer. J. Heat Transf. 131 (12), 121009 https://doi.org/10.1115/1.3220144

Kang M.G., 1998. Experimental investigation of tube length effect on nucleate pool boiling heat transfer, Ann. Nucl. Energy 25 (4-5), 295-304. https://doi.org/10.1016/S0306-4549(97)00056-X

Kang M.G., 2000. Effect of surface roughness on pool boiling heat transfer, Int. J. Heat Mass Tran. 43 (22) 4073-4085. https://doi.org/10.1016/S0017-9310(00)00043-0

Kang K.H., Kim S., Bae B.U., Cho Y.J., Park Y.S., Yun B.J., 2012. Separate and integral effect tests for validation of cooling and operational performance of the APR+ passive auxiliary feedwater system. Nucl. Eng. Technol. 44 (6), 597-610. https://doi.org/10.5516/NET.02.2012.710

Kang S.H., Lee S.W., Kang H.G., 2019. Performance analysis of the passive safety features of iPOWER under Fukushima-like accident conditions. Nucl. Eng. Technol. 51 (3), 676-682. https://doi.org/10.1016/j.net.2018.11.010

Kapitza P.L., 1948. Wave flow of thin layers of viscous liquid. Part I. Free flow. Zhurnal Eksp. I Teor. Fiz. 18, 3-18.

Annals of Nuclear Energy 160 (2021) 108436
https://doi.org/10.1016/j.anucene.2021.108436

Kim S.J., No H.C., 2000. Turbulent film condensation of high pressure steam in a vertical tube. Int. J. Heat Mass Tran. 43 (21), 4031-4042. https://doi.org/10.1016/S0017-9310(00)00015-6

Kral P., 2015. Improvement of RELAP5 models for condensation of steam and steam-gas mixture in horizontal and inclined tubes. In: Proceedings of the 16th International Topical Meeting on Nuclear Reactor Thermal Hydraulics, Chicago, IL, USA, August 30-September 4.

Kuhn S.Z., Schrock V.E., Peterson P.F., 1997. An investigation of condensation from steam-gas mixtures flowing downward inside a vertical tube. Nucl. Eng. Des. 177 (1-3) 53-69. https://doi.org/10.1016/S0029-5493(97)00185-4

Kutateladze S.S., 1963. Heat transfer Theory fundamentals. Atomizdat, Moscow/E. Arnold Publishers, London/ Academic Press Inc, New York.

Lee S.W., Heo S., Ha H.U., Kim H.G., 2017. The concept of the innovative power reactor. Nucl. Eng. Technol. 49 (7), 1431-1441. http://dx.doi.org/10.1016/j.net.2017.06.015

Leiner W., 1994. Heat Transfer by Nucleate Pool Boiling—General Correlation Based on Thermodynamic Similarity. Int. J. Heat Mass Tran. 37 (5), 763-769. https://doi.org/10.1016/0017-9310(94)90114-7

Liu L., Zhang D., Yan Q., Xu R., Wang C., Qiu S., Su G.H., 2017. RELAP5 MOD3.2 modification and application to the transient analysis of a fluoride-salt-cooled high-temperature reactor. Ann. Nucl. Energy 101, 504-515. https://doi.org/10.1016/j.anucene.2016.11.047

Liu L., Zhang D., Song J., Wang C., Gao X., Tian W., Qiu S., Su G.H., 2018. Modification and application of Relap5 Mod3 code to several types of nonwater-cooled advanced nuclear reactors. Int. J. Energ. Res. 42 (1), 221-235. https://doi.org/10.1002/er.3949

Martelli D., Venturini A., Utili M., 2018. Literature review of lead-lithium thermophysical properties. Fusion Eng. Des. 138, 183-195. https://doi.org/10.1016/j.fusengdes.2018.11.028

Mascari F., Bersano A., Alcaro F., Stempniewicz M., Albright L., Jevremovic T., Andrews N., Gauntt R., Austregesilo H., Buchholz S., Bellomo A., D'Auria F., Di Palma G., Lanfredini M., Spina G., Bertani C., De Salve M., Falcone N., Caruso G., Giannetti F., Narcisi V., Choi C., Ha K., Jeon B. G., Kang K. H., Kim K., Park H. S., Karppinen I., Lahovský F., Meca R., Parduba Z., Lien P.H., Tomashchik D. Y., Burgazzi L., Lombardo C., Meloni P., Ferri R., Sandberg N., 2020. OECD/NEA/CSNI/WGAMA PERSEO benchmark results report (under review).

Mascari F., Nakamura H., Umminger K., De Rosa F., D'Auria F., 2015. Scaling issues for the experimental characterization of reactor coolant system in integral test facilities and role of the system code as extrapolation tool. In: Proceedings of the 16th International Topical Meeting on Nuclear Reactor Thermal Hydraulics, Chicago, IL, USA, August 30-September 4.

Marinari R., Tarantino M., Nitti F.S., Alemberti A., Caramello M., Achilli A., Ferri R., Rizzo E., Giannetti F., 2018. SIRIO: An Experimental Facility for a New Heat Removal System Passively Controlled by Non-Condensable Gases. In: Proceedings of the 26th International Conference on Nuclear Engineering, London, England, July 22-26, 2018. https://doi.org/10.1115/ICONE26-82379

McAdams W.H., 1954. Heat Transmission, third ed., McGraw Hill, New York.

Melchiorri L., Narcisi V., Giannetti F., Caruso G., Tassone A., 2021. Development of a RELAP5/MOD3.3 module for MHD pressure drop analysis in liquid metals loops. Submitted to Nucl. Fusion.

Annals of Nuclear Energy 160 (2021) 108436
https://doi.org/10.1016/j.anucene.2021.108436

Narcisi V., Giannetti F., Caruso G., 2019. Investigation on RELAP5-3D© capability to predict thermal stratification in liquid metal pool-type system and comparison with experimental data. Nucl. Eng. Des. 352, 110152. https://doi.org/10.1016/j.nucengdes.2019.110152

Narcisi V., Giannetti F., Caramello M., Caruso G., 2020a. Preliminary evaluation of ALFRED revised concept under station blackout. Nucl. Eng. Des. 364, 110648. https://doi.org/10.1016/j.nucengdes.2020.110648

Narcisi V., Melchiorri L., Giannetti F., Caruso G., 2020b. Assessment of RELAP5-3D for application on in-pool passive power removal systems. In: Proceedings of the 30th European Safety and Reliability Conference and the 15th Probabilistic Safety Assessment and Management Conference, Venice, Italy, November 1-5.

Nishikawa K., Fujita Y., Ohta H., Hidaka S., 1982. Effect of the surface roughness on the nucleate boiling heat transfer over the wide range of pressure. In: Proceedings of the 7th International Heat Transfer Conference, München, Germany.

Nusselt W., 1916. Die Oberflächenkondensation des Wasserdampfes. Z Vereines Deutsch Ing 60, 541-546 569-575.

Papini D., Cammi A., 2010. Modelling of Heat Transfer Phenomena for Vertical and Horizontal Configurations of In-Pool Condensers and Comparison with Experimental Findings. Sci. Technol. Nucl. Ins. 2010, 815754. https://doi.org/10.1155/2010/815754

Pioro I.L., Rohsenow W., Doerffer S.S., 2004. Nucleate pool-boiling heat transfer I: review of parametric effects of boiling surface. Int. J. Heat Mass Tran. 47 (23), 5033-5044. https://doi.org/10.1016/j.ijheatmasstransfer.2004.06.019

Rassame S., Hibiki T., Ishii M., 2017. ESBWR passive safety system performance under loss of coolant accidents. Prog. Nucl. Energ. 96, 1-17. https://doi.org/10.1016/j.pnucene.2016.12.005

Rohsenow W.M., 1952. A method of correlating heat transfer data for surface boiling of liquids. Trans. 74, 969-976.

Rohsenow W.M., Hartnett J.P., Cho Y.I., 1998. Handbook of heat transfer. Third Edition. McGraw-Hill. New York.

Sateesh G., Das S.K., Balakrishnan A.R., 2009. Experimental studies on the effect of tube inclination on nucleate pool boiling. Heat Mass Transfer 45, 1493-1502. https://link.springer.com/article/10.1007/s00231-009-0522-9

Schulz T.L., 2006. Westinghouse AP1000 advanced passive plant. Nucl. Eng. Des. 236 (14-16), 1547-1557. https://doi.org/10.1016/j.nucengdes.2006.03.049

Shah M.M., 1979. A general correlation for heat transfer during film condensation inside pipes. Int. J. Heat Mass Tran. 22 (4), 547-556. https://doi.org/10.1016/0017-9310(79)90058-9

Shah M.M., 1981. Heat transfer during film condensation in tubes and annuli; a literature survey. Ashrae Tran. 87 (1981) 1086-1105.

Shah M.M., 2009. An Improved and Extended General Correlation for Heat Transfer During Condensation in Plain Tubes. HVAC&R Res. 15 (5), 889-913.

Shah M.M., 2013. General Correlation For Heat Transfer During Condensation in Plain Tubes: Further Development and Verification. Ashrae Tran. 119.

Shah M.M., 2016. Comprehensive correlations for heat transfer during condensation in conventional and mini/micro channels in all orientations. Int. J. Refrig. 67, 22-41. http://dx.doi.org/10.1016/j.ijrefrig.2016.03.014

Shumway R.W., 1995. Assessment of MIT and UCB Wall Condensation Tests and of the Pre-Release RELAP5/Mod3.3 Code Condensation Models. Idaho Natl. Lab., pp. 1-40.

The RELAP5/Mod3.3 Code Development Team, 2003a. RELAP5/Mod3.3 Code Manual Volume I: code structure, system models, and solution methods. U. S. Nuclear Regulatory Commission, pp. 1-428. NUREG/CR-5535/Rev P3-Vol I.

The RELAP5/Mod3.3 Code Development Team, 2003b. RELAP5/Mod3.3 Code Manual Volume IV: models and correlations. U. S. Nuclear Regulatory Commission, pp. 1-550. NUREG/CR-5535/Rev P3-Vol IV.

Vierow K.M., Schrock V.E., 1991. Condensation in a natural circulation loop with noncondensable gases, Part I – heat transfer. In: Proceedings of the International Conference on Multiphase, Tsukuba, Japan.

Xiaofan H., Zhongning S., Wenjing L., 2017. Capability of RELAP5 code to simulate the thermal-hydraulic characteristics of open natural circulation. Ann. Nucl. Energy 109, 612-625. http://dx.doi.org/10.1016/j.anucene.2017.06.010

Xing J., Song D., Wu Y., 2016. HPR1000: Advanced Pressurized Water Reactor with Active and Passive Safety. Engineering-London. 2 (1), 79-87. https://doi.org/10.1016/J.ENG.2016.01.017